THIN FILM SYNTHESIS IN COMPOUND OXIDES AND THEIR ELECTRICAL AND MAGNETIC CHARACTERIZATION

A DISSERTATION

Submitted in partial fulfillment of the requirements
for the award of the degree

Of

MASTER OF TECHNOLOGY

In

DEPARTMENT OF METALLUGRICAL AND MATERIALS ENGINEERING

(*with specialization in Industrial Metallurgy*)

By

PRAJU L HADIMANI

DEPARTMENT OF METALLURGICAL AND MATERIALS ENGINEERING
INDIAN INSTITUTE OF TECHNOLOGY ROORKEE
ROORKEE - 247 667 (INDIA)

MAY 2016

CANDIDATE'S DECLAIRATION

I hereby declare that the proposed work presented in this dissertation entitled "**Thin film synthesis in compound oxides and their electrical and magnetic characterization**" submitted by me is in partial fulfillment of the requirements for the award of the degree of **Master of Technology** in **Industrial Metallurgy** in the **Department of Metallurgical and Materials Engineering**, **Indian Institute of Technology Roorkee** is an authentic record of my own work carried out during the period of July 2015 to May 2016 under the supervision of **Dr. Anjan Sil**, Professor and Head, Department of Metallurgical and Materials Engineering, Indian Institute of Technology Roorkee, India. I further declare that the work presented in this dissertation has not been and will not be submitted by me for the award of any other degree in this University or any other University.

Dated: 18-05-2016

Place: Roorkee

Praju L Hadimani

Enroll. No.: 14544014

CERTIFICATE

This is to certify that the above statement made by the candidate is correct to the best of my knowledge and belief.

Dr. Anjan Sil

Professor and Head,

Department of Metallurgical and Materials Engineering

IIT Roorkee, INDIA – 247 667

ACKNOWLEDGMENT

I would first express my sincere gratitude and thanks to my thesis supervisor **Dr. Anjan Sil**, Professor and Head, Department of Metallurgical and Materials Engineering, Indian Institute of Technology Roorkee, India. For the timely support he extended both technically and morally during my M.Tech project work. Prof. Anjan Sil consistently allowed this project as my own and steered me in the right direction throughout this project. He provided enthusiastic motivation for this project work and helped me focus on my ideas and freedom to explore on my own. His support, understanding, expert guidance and fanatical approach towards scientific research always proved effective in keeping me focused towards this project work. Without his patience and timely counsel this project work would have been overwhelming.

I would also like to give my sincere thanks to all members of laboratory. Mr. Sobhit Saxena, Mr. Abhishek Gupta and Mr. Hari Raj for their support, suggestions and goodwill for this project.

Sincere thanks to technical staff of MMED and IIC, IIT Roorkee to helped me at various stages during the project work.

Finally I would like to thank my Mother, Father and Brother for their encouragement support and love for the last two years and my past entire life. I take this opportunity to thank my friends and well-wishers for their support.

ABSTRACT

In this project TM (Transition Metal) doped ZnO thin films $Zn_{(1-X)}Fe_XO$ ($0 \leq X \leq 20$) with molarity 1M were synthesized by sol-gel method and deposited the on glass substrate by spin-coating. Films were synthesized by preheating at 200 ºC for 10 minutes after each coating and annealing at 500 ˚C temperature for 2 hours followed by furnace cooling. Structural, Magnetic and electrical properties of the thin film samples were analyzed by X-ray diffraction (XRD), FE-SEM, SPM (Scanning Probe Microscopy), HRTEM, SQUID (Superconducting Quantum Interference Device), two probe and four probe set up. XRD analysis show that all samples have a wurtzite hexagonal structure and films have preferred orientation along the (101) plane and no secondary phases were present for Fe doping concentration of (0-15 at.%) however for 20 at.% very small amount of secondary phases were detected. As Fe content increases peak intensity decreases and shift towards higher angle (2θ value) side due to c-axis (lattice constant) decreases implying Fe^{3+} (0.68 Å) is successfully substituted at Zn^{2+} (0.74 Å) sites in ZnO lattice. FE- SEM micrographs were used to study the structural, elemental and morphological properties of the thin films and results show that samples are uniform and have a homogeneous surface distribution of grains. By increasing the Fe concentration in ZnO the particle size of the thin films were decreased. Magnetic properties of the samples have been studied by SQUID, M-H curves (300K) and M-T curves (5K – 330K), the analysis revealed that samples have M – H curves with a small saturation magnetization (M_s) and remanence magnetization (M_r), which indicates the Room Temperature Ferromagnetic (RTFM) properties. M-T curves show for Fe (0-20 at.%) all samples have positive M_s (saturation magnetization) i.e. ferromagnetic properties and for Fe (20 at.%) small amount of secondary phases were detected. Topographical analysis and roughness were determined by SPM. The results show film growth is along c-axis i.e. perpendicular to the substrate and as the Fe doping increases the roughness of the films decreases. Two probe method is used for V-I characteristics and Four probe set used to determine the Resistivity (ρ) and Activation energy (E_A) of the thin films.

***Key words*:** Thin films, Spin-coating, Sol-gel, RTFM, Saturation Magnetization, Resistivity (ρ), Activation energy (E_A).

Contents

List of Figures

1 INTRODUCTION

1.1 Introduction

First DMS (Dilute Magnetic Semiconductors) material was discovered in the year 1995-1996 by Ohne et al by Molecular Beam Epitaxy (MBE) method. In 2000-2001 Dietl et al theoretically predicted that Curie temperature T_c of p-type semiconductors could be increased above room temperature and in 2001 experimentally discovered by the Metal Organic Chemical Vapor Deposition (MOCVD) technique with a high Curie temperature up to T_c= 800 K and theoretically T_c = 940 K [1][15]. A DMS is compound having properties in between magnetic element and a non-magnetic semiconductor. DMSs are synthesized by doping a non-magnetic semiconductor with TMs (Transition Metals) like V, Cr, Fe, Mn and Ti etc. Recently TM doped ZnO have gained considerable attention in various fields due to their application in modern technology, especially in spintronics and have good physical properties.

Since the past decade the application of DMSs has increased considerably due to applications of electronic devices by adding spin of electrons in addition to their charge. The DMS based spintronics are widely used in magnetic recording devices and they give excellent result. ZnO is n-type semiconductor with a wide band gap (3.37 eV at RT), low cost, abundant, nontoxic and a large excitation bonding energy also they have excellent optical, physical, chemical and electrical properties [1] [2]. They used in gas sensors, solar cells, transparent electrodes, transducers [3]. Because of various good properties and potential applications of ZnO in modern technologies, during past recent years more attraction has been paid towards research on TM doped ZnO [4].

DMSs are solid solutions in which a small percentage of cations are replaced by magnetic impurities like TMs. Most of the DMSs have low T_c and this limitation of DMSs has disadvantage in practical applications. T_c of DMS can be increased above the room temperature for a p-type DMSs, because of wide band gap semiconductors like ZnO and GaN Ferromagnetism was stable in DMSs. The origin of RTFM in DMSs is still a matter of debate that is either TM^{2+} replacement of Zn^{2+} (carrier mediated exchange) or the secondary phase formation. DMSs are potential candidates for future spintronics like spin polarized information storage and processing devices.

Now Days, the most research are focused on synthesis of RTFM semiconductors, by addition of impurities like multivalent or TM metals into ZnO lattice system. This has been an important alternate strategy to attain RTFM with a high T_c. When ZnO is doped or co-doped with TMs position, magnetic property and possession of Fermi level can be altered by the *d* shell electrons of the TM ions. Because of these reasons the most investigations are concentrated on knowing the interaction of magnetic properties in the TM doped ZnO.

However most of the experimental results have shown enhancement of ferromagnetic properties, transition to FM from PM (Paramagnetic) and also some analysis revealed decrease in the FM behavior of TM doped or co-doped ZnO. [31]

In this project, we have developed a simple and easy way towards the synthesis of $Zn_{(1-X)}Fe_XO$ by sol-gel method at room temperature. The morphological, structural and topographical characterizations were analyzed by XRD, FE-SEM, SPM and TEM. The magnetic characterization was done by SQUID and electrical properties were studied using two probe and four probe set up. The oxidation state (Fe^{2+} or Fe^{3+}) of the Fe dopant in the ZnO lattice was revealed by the intensities and shifts in the peaks of XRD patterns of the $Zn_{(1-X)}Fe_XO$.

1.2 Basic principle of RTFM

Several theoretical calculations and experimental work have been performed to explain the RTFM. The proposed mechanisms include (BMP) Bound Magnetic Polaron mechanism which involving defects such as Zn interstitials (Zn_i), Oxygen vacancies (V_o) and formation of FM secondary compounds like Fe clusters, FeO, Fe_2O_3, Fe_3O_4 etc.

Basically there are two approaches to understand the RTFM in DMSs

- Mean field theory (Zener model).
- Clusters formed by the doped or co-doped magnetic atoms are that responsible for ferromagnetism.

1.3 Thin Films

Thin film is a layer of material with a thickness varies from nanometer to several micrometers to nanometer. It could be monolayer, multilayer, amorphous, crystalline, microcrystalline, junctions, supported, freestanding etc.

Thin Films have different properties than the bulk materials from which they have made of and their properties quite depend on process parameter, substrate used, dopant and manufacturing technique employed for their fabrication. Process parameter includes type of dopant, its solid solubility, its composition, purity, Film growth, film thickness, type of substrate, deposition rate, pre-heating, annealing temperature etc. There are several methods to synthesize TM doped ZnO thin films including techniques used to fabricate the thin films.

1.3.1 Application of thin films

- Mirrors, Lenses, Filters
- Spintronics
- Electrode surfaces
- Photoelectric devices, Solar cells
- Catalyst surface
- Information storage, magnetic, optical memories. etc…

1.4 Compound Oxides

Substances or compounds which react with oxygen in presence of the air and produces its oxide compounds. The oxygen is present in these compound as oxide ion (O^{2-}). There are mainly two categories of compound oxides.

- Metal oxides
- Non-metal oxides

1.4.1 Metal oxides

A metallic compound reacts with oxygen in the air producing its oxide. Metal oxides – 75% of the elements in the periodic table are metals, group 1-12 including alkali metals, transition metals and alkali earth metals along with lanthanides and actinides form ionic oxides i.e. the compounds which contains oxygen as O^{2-} (anion) with the bonds in the nature of covalent. Example – ZnO, MnO_2, K_2O, MgO, CaO etc. Metals have maximum atomic radius, hence they have low electronegativity and ionization potential. Since ionization potential is low they can easily lose their electron/electrons therefore good conductor of electricity and heat.

The metal oxide includes transitional metal oxides i.e. d – block elements group 3-12. They have variable oxidation states; hence can form different types of compounds like Cr_2O_2 and CrO_2. But Cr_2O_2 is metal oxide and CrO_2 is a non-metal oxide. Highest oxidation state of TM is sum of the number of electrons in the *s* orbital and unpaired electrons in the *d* orbital.

For example – V (Z=23) electron configuration $4s^2\ 3d^3$, oxidation states – 2+, 3+, 4+ and 5+
Fe (Z=26) electron configuration $4s^2\ 3d^6$, oxidation states – 2+ and 3+.

1.4.2 Non-metal oxides

Non-metals react with O_2 as oxide ion (O^{2-}) presence of air and produce nonmetal oxides such as NO, N_2O, CO, CO_2, SO_3 etc. The nomenclature has two words, first Greek prefix followed by nonmetal and second oxide, like carbon dioxide, dinitrogen trioxide etc.

The main difference between metal oxides and nonmetal oxides is, metal oxides are solids at RT and are bases, i.e. form alkali solution when dissolve. Nonmetal oxides are usually in gaseous state at RT and form acidic solution when dissolve in water.

1.5 Crystal structure of ZnO

The zinc oxide has wurtzite hexagonal crystal structure belongs to space group P63mc. ZnO is II-IV semiconductor having ionicity between covalent and ionic and E_g=3.36 eV. It is a Hexagonal wurtzite structure with each anion (O^{2-}) is surrounded by four cations (Zn^{2+}) and vice versa at the tetrahedron corners. The tetrahedral positioning has CN = 4 and typical sp^3 covalent bonding between Zn and O atoms.

ZnO is strictly wurtzite hexagonal packing and crystal structure does not changes with physical and chemical conditions. Unlike ZnS which has both wurtzite (HCP), zinc blende (sphalerite) which is cubic packing and cubic Rocksalt. Lattice parameters of ZnO $a = b$ = ~3.2496 Å, c ~ 3.2151 Å with c/a ratio in the range 1.633 – 1.593 and α = β = 90° and γ = 120°. Depending on the type of substrate it was grown on the strain varies like no substrate (minimum), glass (moderate) and quartz (high).

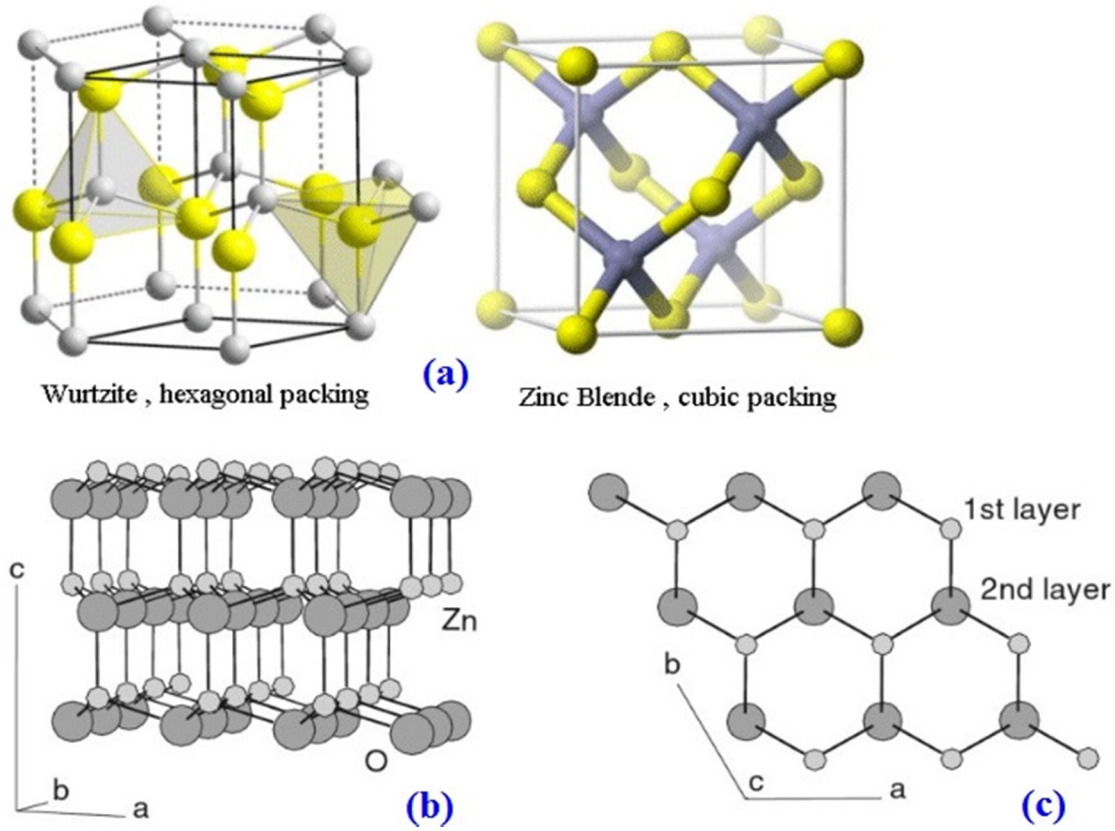

Figure 1.5.1 (a) Wurtzite and cubic structure (b) top Zn atoms end, bottom O atoms end layers (c) ZnO structure along c-axis

ZnO at high temperature experiences solid state reaction i.e. calcination. Also when it is exposed to ambient atmosphere it absorbs water vapor carbon dioxide from the air producing Zinc carbonate ($ZnCO_3$). ZnO is amphoteric i.e. it undergoes reaction with acids and alkalis, the reaction with acids results in zinc sulfate and with alkalis metals it forms zincates. Different ZnO nanostructures can be synthesized by using various processing methods, like nanorods, nanowires, nanocombs, nanocages and nanoparticles etc. Therefore ZnO has probably more number of nanostructure families among all the materials.

The bond length Of Zn-O is 1.9767 Å with a corresponding radius of Zn^{2+} 0.74 Å and 1.40 Å for O^{2-} having ionic bond between them. The bond length (Zn – O) along c – axis is (1.988 Å) higher than along *a* or *b* axis (1.974 Å) [23]. Hence these properties preferentially accounts for formation of hexagonal wurtzite structure than the zinc blende cubic structure. The coefficient of thermal expansion at 300 °C parallel to c – axis is $4.31X10^{-6}$ K^{-1} and normal to c – axis it is $2.49X10^{-6}$ K^{-1} [23].

1.6 Deposition Techniques for synthesis of thin films

There are mainly two classifications of deposition techniques

1.6.1 Chemical Vapor Deposition (CVD)

Chemical Vapor Deposition (CVD) is similar to the PVD, on a vapor source. The main difference between PVD and CVD is in PVD the layer formation is based on a physical condensation process but in CVD it is a chemical reaction mechanism. This process is used to produce high purity and high performance solid materials. The combination of reactive deposition and diffusive transport makes the CVD process better suitable for highly conformal 3-Dimensional deposition.

1.6.2 Physical Vapor Deposition (PVD)

PVD technique is used often for all-solid-state thin-films. In PVD process a vapor is formed of metal by the resistive heating at low pressures that subsequently condensates onto a substrate. Physical methods produce the atoms which are deposited on the wafer or substrate by evaporation and sputtering. There are other methods for thin film synthesis including Spin coating, Dip coating, Spray pyrolysis Magnetron sputtering (DC or RF), Laser ablation, Vacuum evaporator etc.

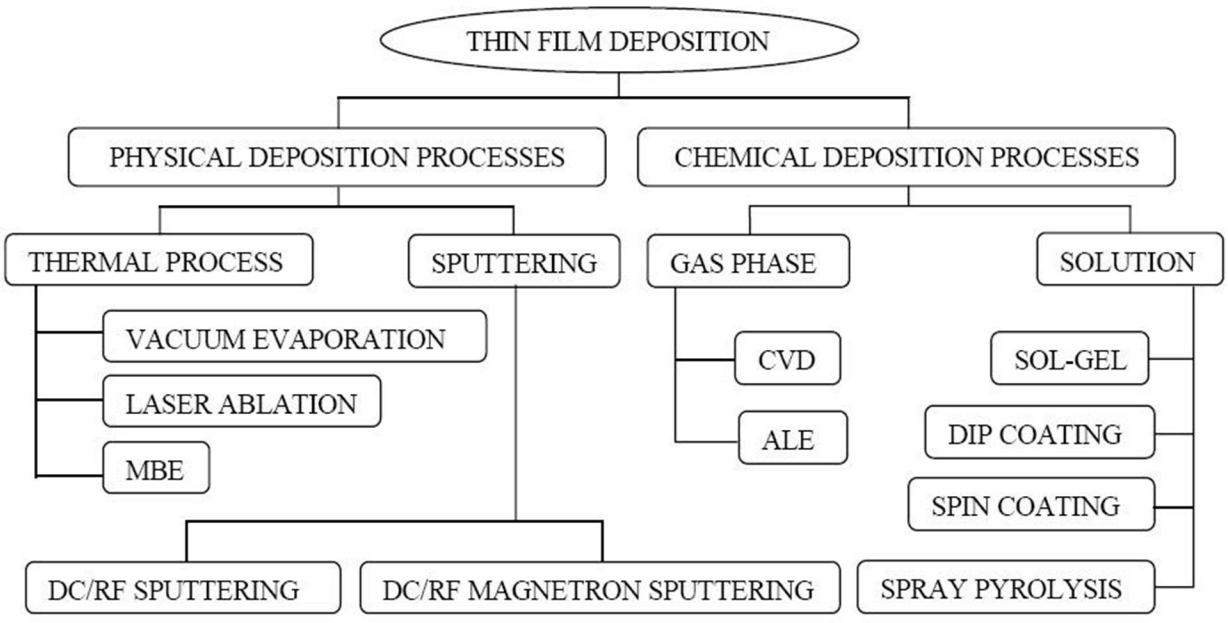

Figure 1.6.1 Thin film deposition techniques [11]

2 LITERATURE SURVEY

This literature survey deals with method for the synthesis of synthesis of thin films by sol-gel technique in which a ZnO matrix is doped with Fe atoms exhibited ferromagnetic ordering. In this method of producing DMS our aim is to attain RTFM, increase Curie temperature T_c the room temperature, higher Magnetization value, achieving good electrical (low resistivity, high conductivity) properties.

Diet et al [1] in 2000-2001 theoretically predicted T_c of the p-type DMSs can be increased above the room temperature. This is because of the ZnO and GaN semiconductors have wide energy band gap of the order of 3.3 eV ferromagnetism was stable in DMSs.

K. Sato and K. Yoshida et al [16] theoretically demonstrated that a TM atoms like, Mn, V, Ni, Fe and Cr doped in ZnO exhibited FM by using first principle calculations. This led to experimental attempts for the preparation of DMSs.

K. Ueda et al [17] soon after the theoretical of RTFM, the experimental reports also resulted in intrinsic RTFM when ZnO and TiO_2 are doped with TMs. These results support lot of experimental and theoretical work on RTFM, DMSs and DMOs and an impulse to know the mechanisms involved for the better materials

S.A. Wolf et al [18], I. Zutic et al [19] TMs doped ZnO have increased due to their hopeful future success applications in the field of spintronics, which tends to increase the properties and applications of the electronic devices by the addition of spin of electrons along with their charge.

L. Znaidi [11] in 2003 they have studied the Sol–gel method of ZnO thin films. Considerable analysis have been done on the preparation and development of ZnO thin films aiming various applications. In this research major work has been done on the oriented films and the growth direction of grains which is oriented along the (0 0 2) direction i.e. normal to the substrate surface.

Huilian Liu et al [21] successfully synthesized the Fe (3%) doped ZnO nanoparticles by sol-gel method, and analyzed the structural and magnetic properties at various Fe concentrations. Magnetic measurements indicated that ZnO/Fe powder was room temperature ferromagnetic.

The analysis also shows that the observed RTFM powder was an intrinsic property of Fe doped ZnO. They found Fe^{2+} and Fe^{3+} states in the doped ZnO powder samples and T_c = 375 K

Muneer M. Ba-Abbad et al [22] in this research powder of ZnO was prepared by doping varying the concentration of iron ions (Fe^{3+}) by sol-gel technique. The structural analysis of Fe doped ZnO was studied. The lattice parameters of Fe doped ZnO nanoparticles were found to be smaller than those of ZnO. This confirms the Fe ions were successfully substituted into the host ZnO lattice without altering its hexagonal (wurtzite) structure. Also the peaks of Fe doped powder were shifted towards higher value of 2θ consistently with increase in Fe^{3+} due to change in the average size of the crystal. The particle shape found to be spherical and optimum Fe^{3+} doping content in ZnO was 50 wt.%.

Debjani Karmakar et al [23] in 2007 they have studied the structural and magnetic properties of TM doped ZnO powder was synthesized by sol-gel technique. They used Zinc acetate hex hydrate and Ferric nitrite Nanohydrate. The XRD results show wurtzite (hexagonal) structure and FWHM of the peaks were increased with increase in the Fe content. The magnetic analysis shows particles exhibits room temperature ferromagnetism. Results also indicate that Fe cations present in Fe^{2+} and Fe^{3+} states. This paper suggest hole doping is crucial for promoting RTFM.

Mariani A. Ciciliati at al [24] In this sol–gel method was used to synthesize the Fe-doped ZnO nanoparticles. TEM analysis revealed hexagonal nanoparticles. As the iron doping in the ZnO increases the average crystallite size of the samples decreases consistently.

Goktas et al [25] in 2013 they have synthesized the $Zn_{(1-X)}Fe_XO$ thin films were prepared by doping different Fe (X= 0-0.20) concentration by using sol-gel dip coating technique. Magnetic analysis show films exhibits ferromagnetic properties at 5 K and 100 K, diamagnetic properties at 200 K and 300 K at a Fe concentration of 0.2%. The results show decrease in the grain size as the Fe dopant increases at Fe 21 at.% secondary phases were started to form.

3 PLAN OF WORK

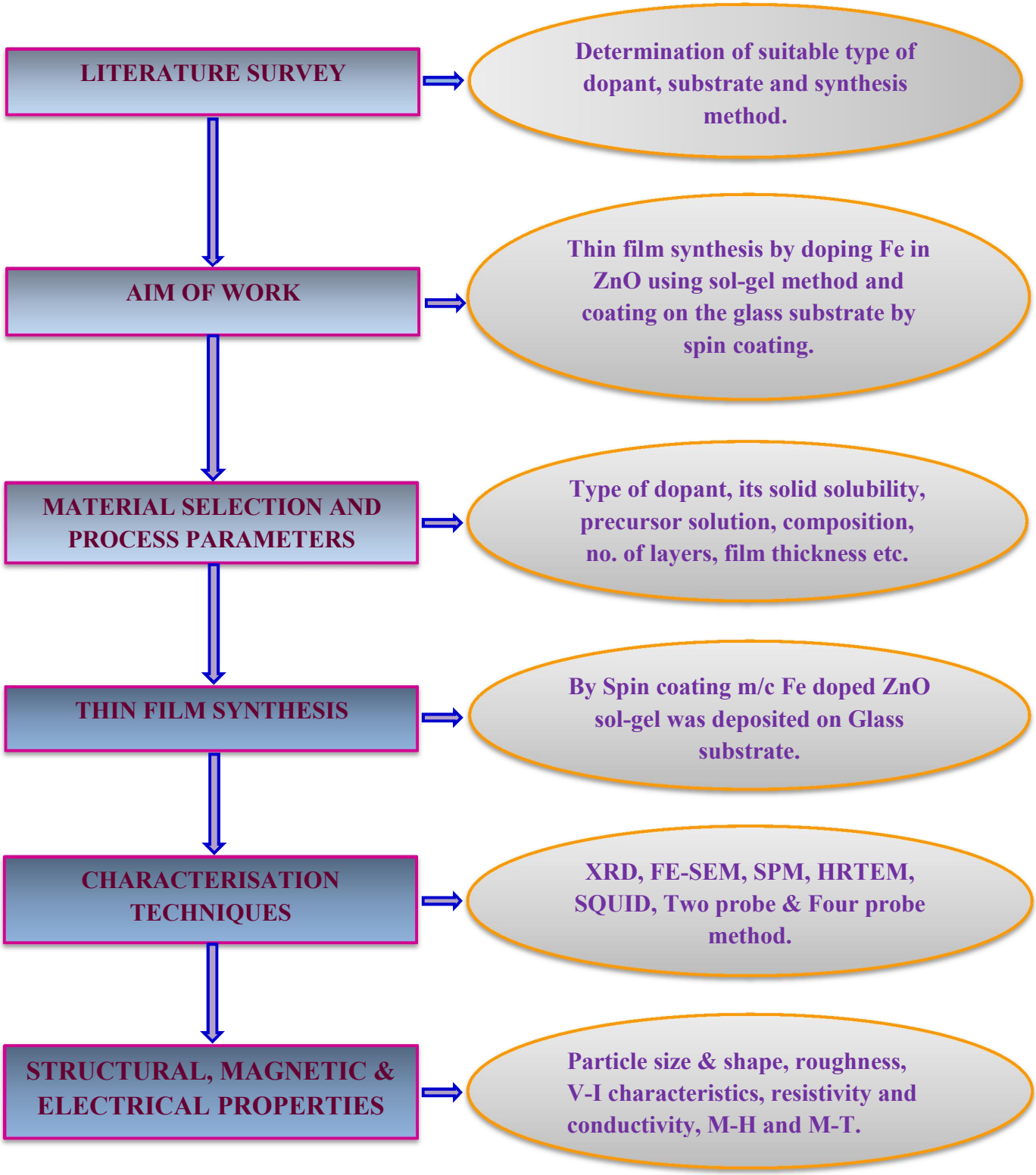

Figure 3.1.1 Flowchart showing plan of work

4 EXPERIMENTAL DETAILS

Thin films of Fe doped ZnO were synthesized by sol-gel method and coated on the glass wafer by spin-coating method. All the chemicals used in this experiment were purchased from Rankem and Sigma Aldrich Company. $Zn_{(1-X)}Fe_XO$ (X = 0 – 20 at.%) with molarity 1M thin films were synthesized by using Zinc Acetate Dehydrate (ZAD) Zn $(CH_3COO)_2 \cdot 2H_2O$ (99.9%) and Ferric Nitrate Nanohydrate (FNN) $Fe(NO_3)_3 \cdot 9\ H_2O$ (99.9%) as a starting materials. These two powders are separately dissolved in 2-Methoxyethanol (1M) after stirring for 1 hr. both the solutions were thoroughly mixed and stirring was continued for 3 hr. at room temperature. To this solution 40 drops of Monoethanolamine (MEA) stabilizer was added drop wise until the solution became transparent and uniform. The precursor solution was aged for 24-36 hours and then deposited on glass substrate using Spin-coating machine (1000-3000 rpm, in steps of 500 rpm for 30s each steps). Synthesized films were pre-heated to 200˚C for 10 min. after each coating to relieve the organic residuals and evaporate the solvent. This procedure was repeated depending upon the final number of layers and thickness needed. The films were then annealed to temperatures of 400 -700˚C for 2 hr. in air as a secondary heat treatment and the films were allowed furnace cooling.

4.1 Sol-gel process

The process is based on the hydrolysis and condensation reaction of orgo-matallic compounds in alcoholic solutions. There must be a chemical bonding between film (ZnO) and the substrate (glass) for the formation of sol-gel coatings on the substrate. The adhesion of oxide coating film to the oxide substrate is achieved by formation of chemical bonds [-M–O–M^1-] on heating to higher temperature. The formation of [-M–O–M^1-] bonds at higher temperature is easier when more number of M – OH and M^1 – OH groups present at the contacting surface of the film and substrate. There are mainly two steps in the of sol-gel process.

Hydrolysis: In this step metal alkoxide [M – OR], where is an alkyl group (R= C_nH_{2n+1}) reacts with water [H_2O] to form metal hydroxide [M – OH]

Condensation: In this process two metal hydroxide [M – OH + HO – M^1] combines to give metal oxide species [M – O – M^1] and water [H_2O] is rejected. Where – M – metal ions in the film and M^1- metal ions in the substrate.

4.2 Sol-gel method of thin film synthesis

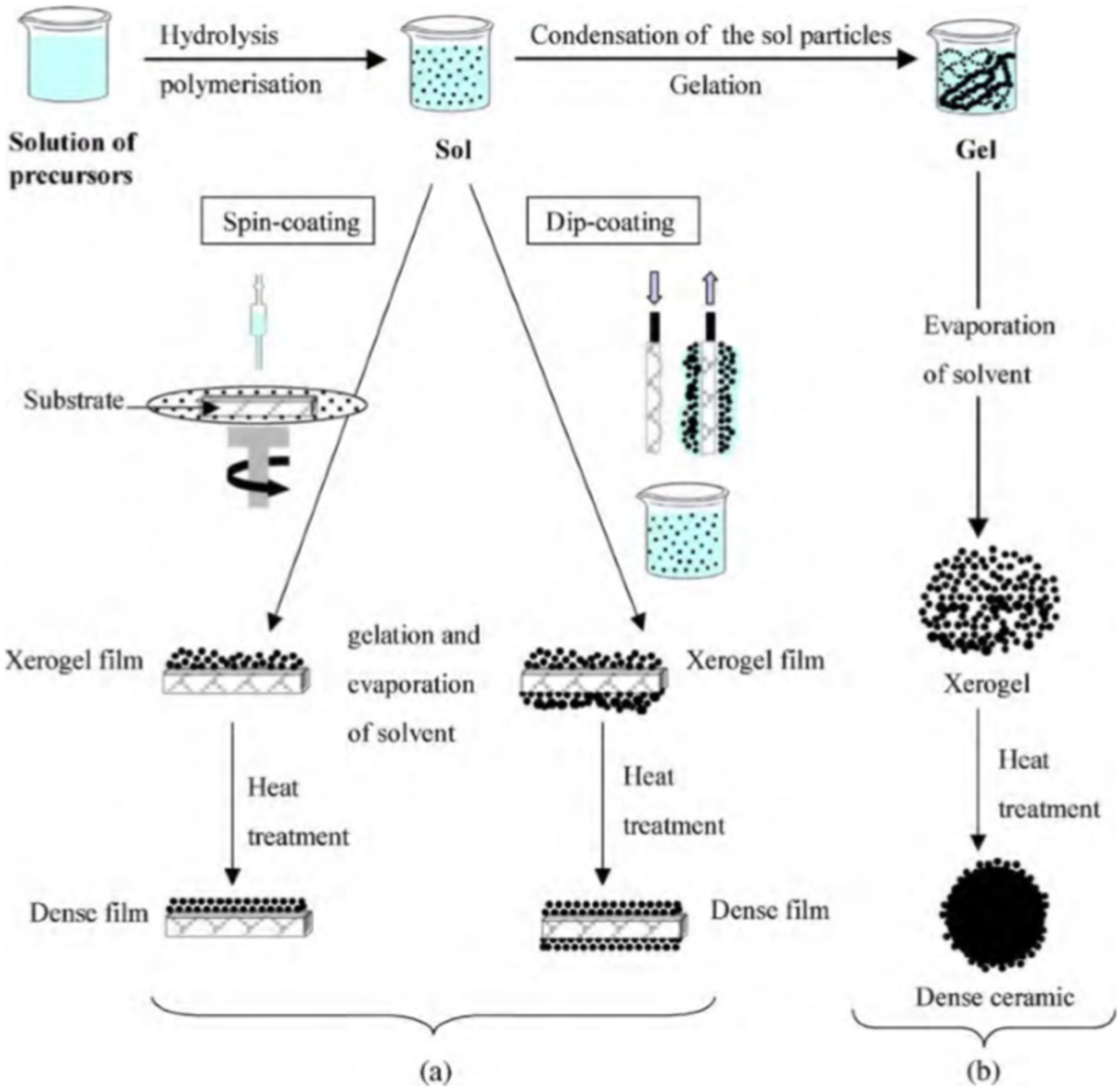

Figure 4.2.1 Schematic diagram showing two types synthesis by the sol–gel method (a) films from a colloidal sol (b) powder from a colloidal sol transformed into a gel. [11]

4.2.1 Advantages of Sol-gel method

- Low temperature method that are organic and inorganic
- Excellent control of the stoichiometry of precursor solution
- Ease of compositional modification
- Relatively low annealing temperature
- Deposition on large substrate area
- Simple and low cost equipments

4.2.2 Applications of Sol-gel method

- Optical coating
- Mirrors, Lenses, Filters
- Clinical and analytical chemistry
- Batteries
- Photoelectric devices, Solar cells
- Catalyst surface
- Information storage, magnetic, optical memories. etc.

Camera Lens

Optical Mirrors

Optical Filters

Solar Panels

Optical Discs

Gas Sensor

Figure 4.2.2 Applications of thin films

4.3 Flow diagram of Sol-gel method of thin film synthesis

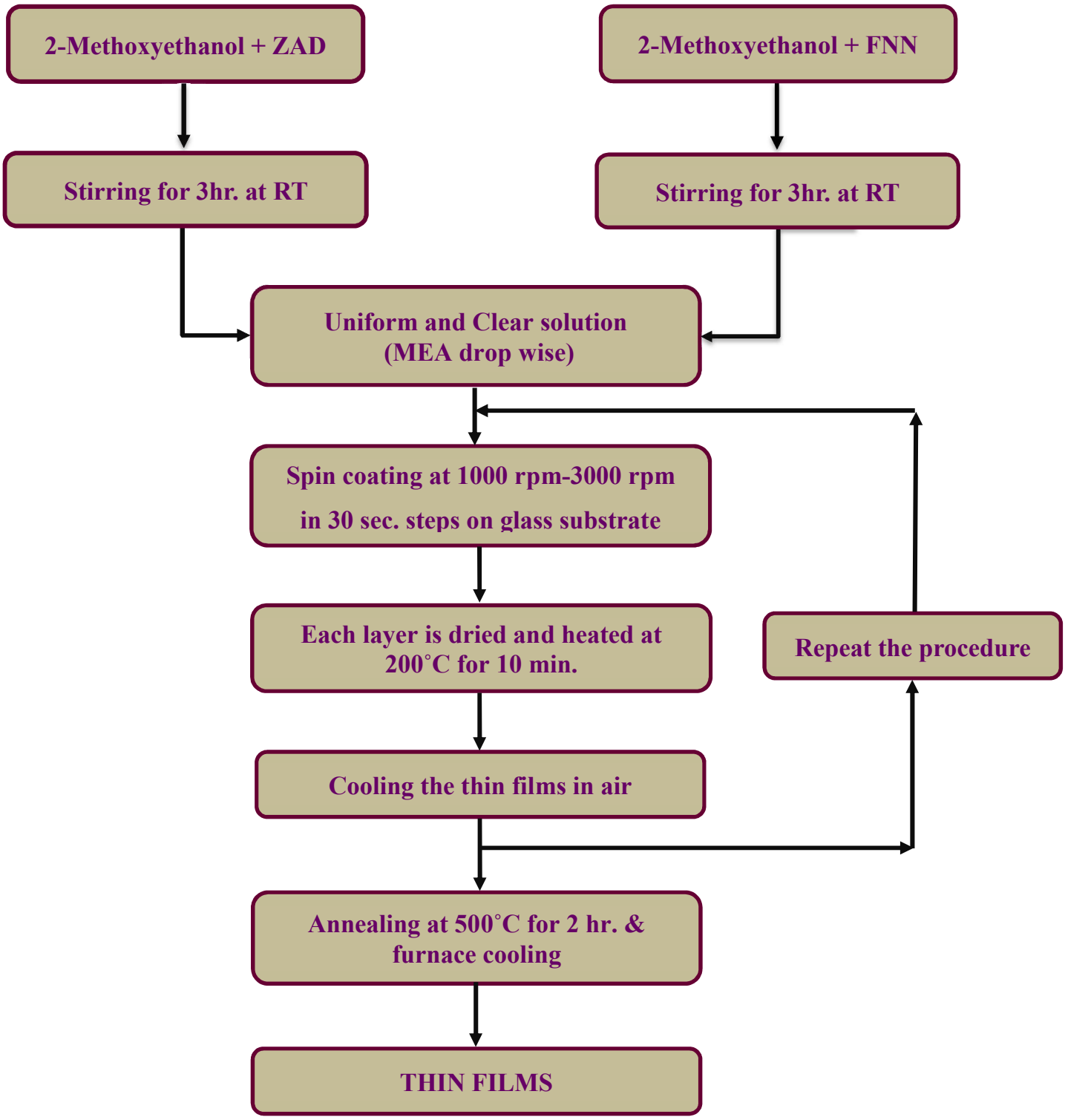

Figure 4.3.1 Flowchart of thin film synthesis

4.4 Phase diagram of ZnO and FeO

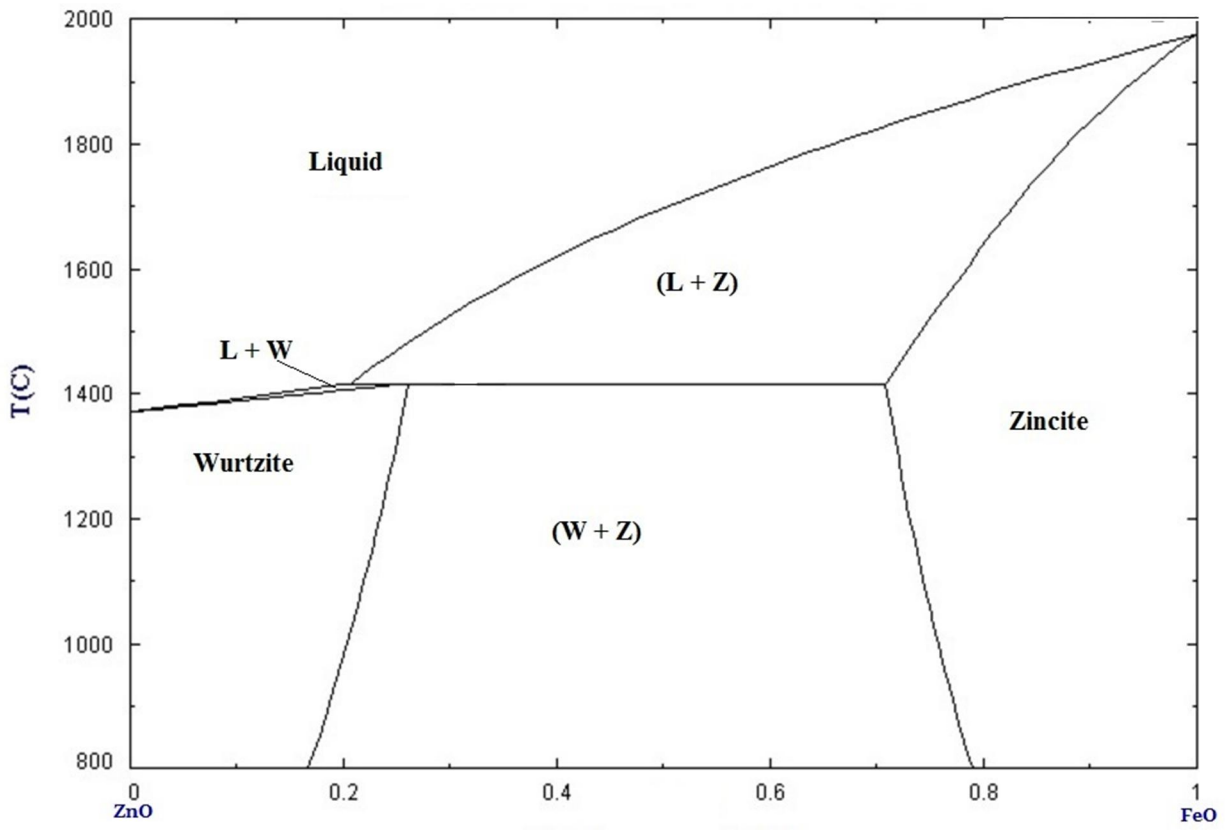

Figure 4.4.1 Binary phase diagram of ZnO & FeO [23]

Figure 4.4.1 shows the binary phase diagram of FeO – ZnO. The peritectic reaction is at ZnO 22 % and at temperature 1410 °C where liquid and solid (zincite) will form another solid i.e. Wurtzite (hexagonal structure). The rock salt $Zn_{(1-X)}Fe_XO$ coexists with hexagonal wurtzite (ZnO) structure up to 800 °C and ZnO 18%. The complete dissolution of wurtzite ZnO depends upon initial stoichiometry of the mixture.

4.5 Precursor solution preparation

The precursor $Zn_{(1-X)}Fe_XO$ (x=0.05 – 0.20) were prepared by using Zinc Acetate Dehydrate (ZAD) and dopant Ferric Nitrate Nanohydrate (FNN) in a solvent 2-Methoxyethanol (2-ME) with a concentration of 1 mole/L using magnetic stirrer. ZAD and FNN were first dissolved in 2-ME at room temperature by using magnetic stirrer after 4 – 5 hrs. both the solution were mixed and stirring was continued. In the meantime MEA sol-stabilizer was added drop by drop until

solution becomes clear and homogeneous according to appropriate MEA to zinc molar ratio calculations.

The atomic percentage of Fe^{3+} in the ZnO sol were 0%, 5%, 10%, 15%, 20%. The prepared ZnO sols were kept at room temperature about 24-36 hours for aging. Then Fe doped ZnO thin films were coated on the glass substrate by using spin-coating equipment.

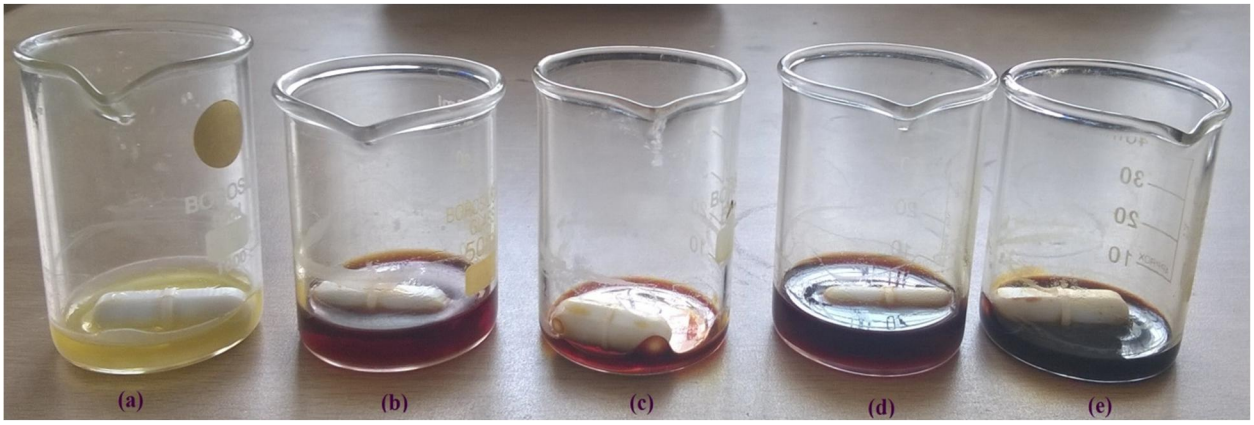

Figure 4.5.1 ZnO sols with a Fe (a) 0 at.% (b) 5 at.% (c) 10 at.% (d) 15 at.% (e) 20 at.%

Figure 4.5.2 Spin NXG spin coating equipment with vacuum pump

Table 4.1 Amount of ZAD and FNN used for sol preparation with 1M for $Zn_{(1-X)}Fe_XO$

Fe (at.%)	ZAD (gm)	FNN (gm)	2-ME (ml)	MEA (ml)
0	2.6964	0	12.285	0.7371
5	2.5767	0.2496	12.356	0.7043
10	2.4554	0.5021	12.4285	0.6712
15	2.3326	0.7576	12.50	0.6491
20	2.2084	1.0161	12.58	0.6036

4.6 Thin Film synthesis

The substrate material used was glass slides of Soda lime (softening temperature 545 °C) and ITO coated (softening temperature 725 °C) having a dimension of 1" x 1" with1 mm thickness. Before spin-coating the slides were washed thoroughly with Ethanol solution to remove moisture grease dust etc. the duration time for each layer was 90 sec. from 1500 rpm-2500 rpm (500 rpm in steps for30 sec.). After each layer the coated glass slide was place inside the oven at 200 °C for 10 min. in the presence of air for pre-heating. The procedure from spin-coating to pre-heating treatment was repeated several times depending on the number of layers or thickness required. Altogether two samples of each doping concentrations were prepared with a same spin-coating speed, pre-heating temperature and time. All the samples were annealed at 500 °C in air for 2 hours in the furnace and allowed furnace cooling (12hr. – 14hr.). The annealed samples were used for structural, magnetic and electrical characterization.

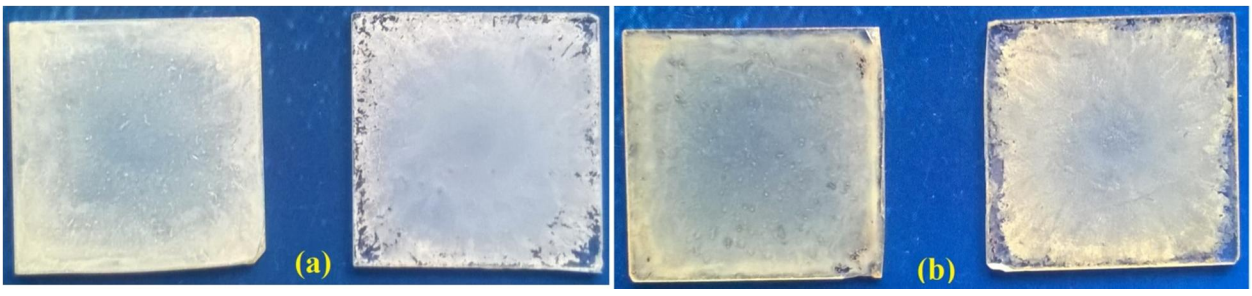

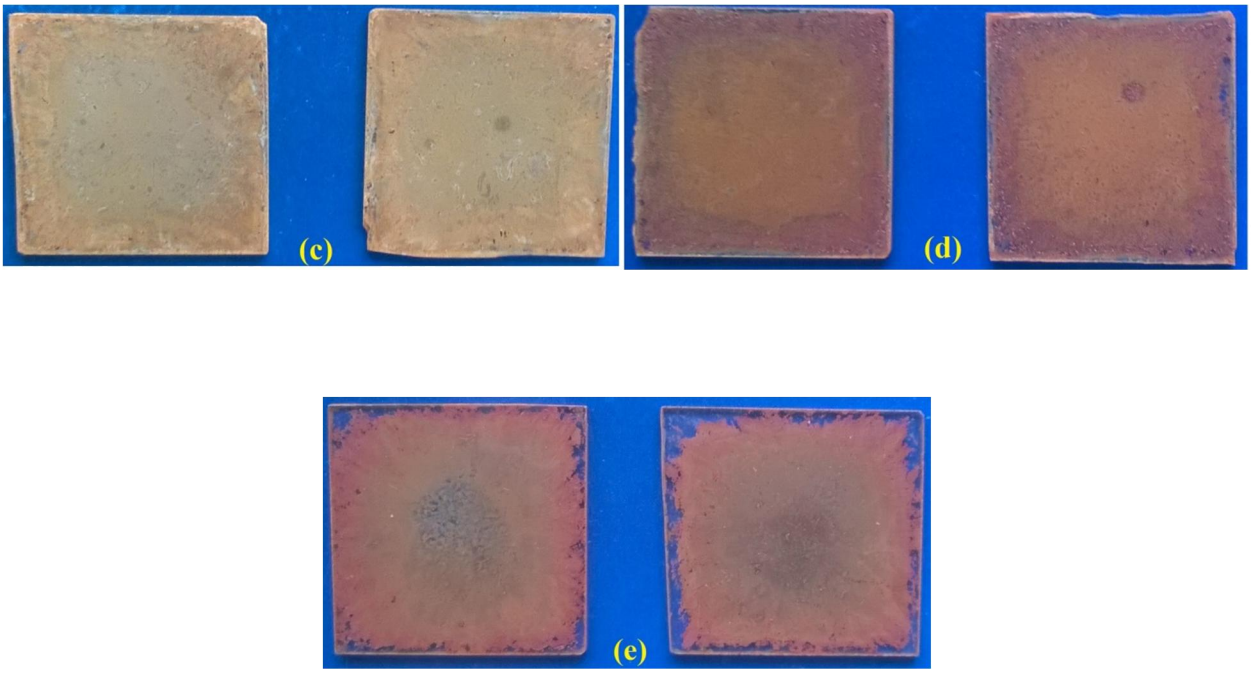

Figure 4.6.1 Fe doped ZnO coated thin films (a) 0 at.% (b) 5 at.% (c) 10 at.% (d) 15 at.% (e) 20 at.%

Figure 4.6 shows $Zn_{(1-x)}Fe_xO$ (0-20 at.%) Thin films coated on the glass substrate with a dimension of 1" x 1". We can also see that as the Fe doping concentration increases the films become more brownish color this is because the FNN is brownish in color.

4.7 X-Ray Diffraction (XRD) Technique

X-ray diffraction (XRD) is used in crystallography as an analytical technique mainly used for phase identification of a crystalline materials. XRD is also used for determining crystal structure, lattice constants, lattice strain, and compositions of unknown materials.

Inter planer spacing (d) can be calculated by plotting Intensity (a.u.) of diffracted radiation vs scanning angle 2θ. By using Bragg's law

$$\mathbf{2d\sin\theta = n\lambda} \quad \text{———} \quad (4.1)$$

Where n – reflection order

θ – Bragg angle

λ – Wavelength of incident radiation (in this case Cu Kα)

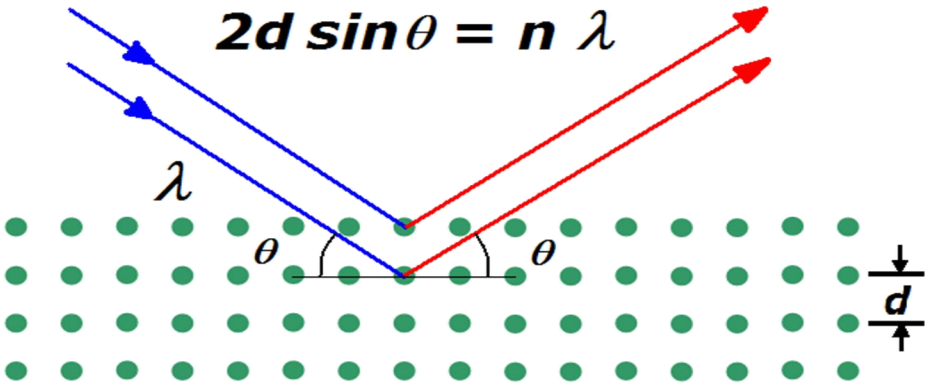

Figure 4.7.1 Schematic diagram of Bragg's Reflection

Also crystalline size can be calculated using Debye-Scherrer equation

$$D = \frac{K\lambda}{\beta \mathrm{Cos}\,\theta} \qquad \text{(4.2)}$$

D = Mean size of the crystalline

K = Dimensionless shape factor and has a typical value of 0.94

λ = X-ray wavelength used (Copper K_α = 1.5406 Å)

β = FWHM (width of the peak at half the maximum intensity) in radians

θ = Diffraction angle

4.7.1 Lattice strain

Lattice strain (ε) of Fe doped ZnO and pure ZnO was calculated by the formula. [22]

$$\varepsilon = \frac{C - C_o}{C_o} \qquad \text{(4.3)}$$

C – Lattice parameter of the Fe doped ZnO (from XRD)

C_o – Lattice parameter of the bulk ZnO

4.8 Field Emission Scanning Electron Microscope (FE-SEM)

FE-SEM produces high resolution images of a sample by scanning with focused beam of electrons. High energy electrons are used to see the object at a very fine level. In standard scanning electron microscopes, electrons are generated from tungsten filament when it is heated. But in FE-SEM instead of light FE-SEM works with electrons which are liberated by field emission from the conductor due to strong electric field between cathode and the anode. The electrons interact with the atoms on the surface of a sample and producing information about the surface topography and composition. Compared to modern optical microscopes FE-SEM have advantages such as large resolution, magnification is very high (up to 500000 X), depth of focus is large, gives high quality images and sample preparation is easy. Using FE-SEM we have analyzed the morphology and particle size of the Fe doped ZnO thin films.

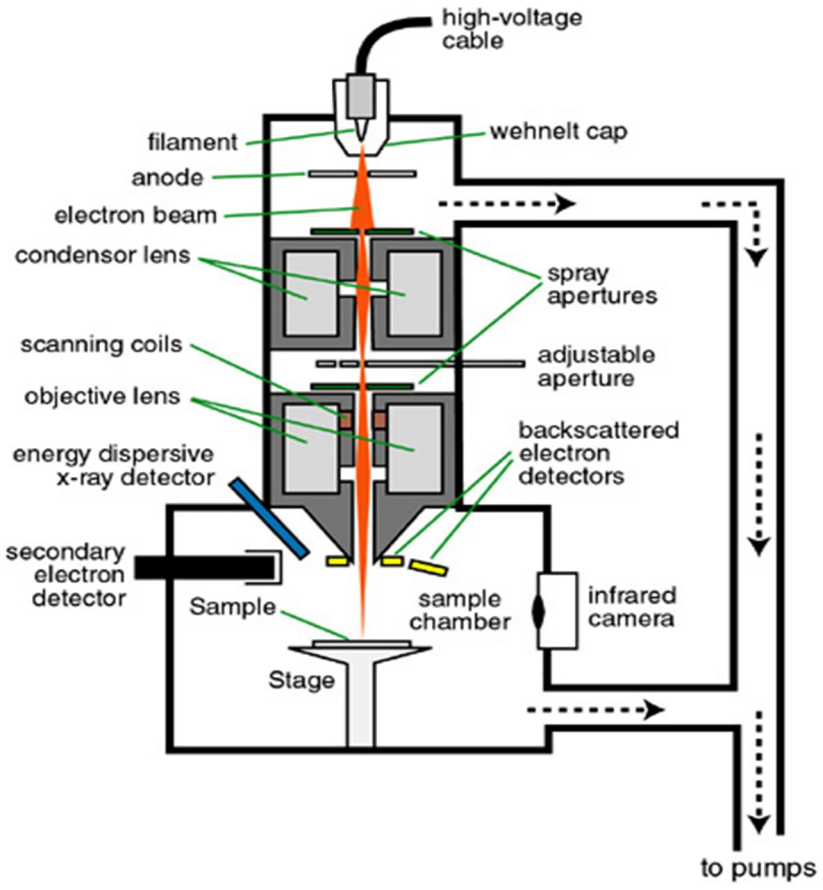

Figure 4.8.1 Schematic diagram of FE-SEM [32]

4.9 Scanning Probe Microscopy (SPM)

SPM is a branch of microscopy that generates the images of the surfaces using physical probe which is in contact with the surface of the specimen to be scanned. The image is generated, line by line mechanical movement of the probe in a raster scan of the specimen and recording the probe-surface interaction as a function of position. Important types of the SPM are – AFM, FMM, MFM, EFM and STM etc. The sample is mounted on the piezoelectric scanner, the PTS provides the 3D positioning.

To achieve accuracy close to atomic scale 3 components are essential

- A cantilever and a sharp magnetic tip (1 Å)
- A scanner for controlling x, y and z position
- Feedback mechanism

4.9.1 Applications of SPM

- For obtaining 3D topographic images of both insulators and conductor.
- It can operate in fluid, gas and ambient environments and can measure elasticity, roughness, hardness, friction and adhesion.
- Used for the samples including atoms, molecules and biological species like DNA, cells and proteins.

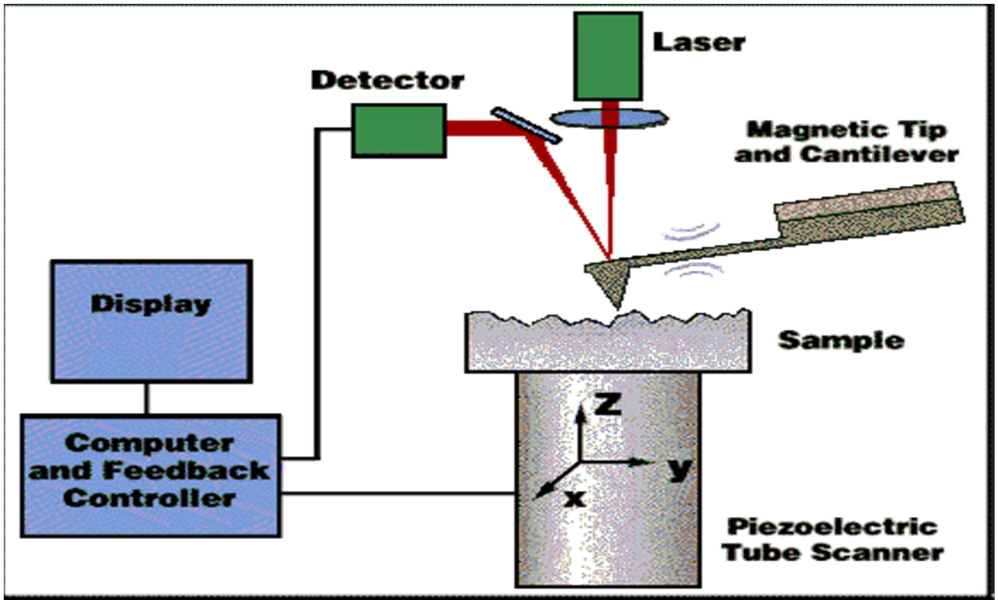

Figure 4.9.1 Schematic diagram of SPM [33]

4.10 Electrical Characterization

4.10.1 V-I Characteristics of Thin Films

ITO coated borosilicate glass slides are used for the electrical characterization. Thin films were deposited on the conductive side of the slide and V-I characteristics were determined by Two probe set up KEITHLEY 2400 source measuring unit. The digital multimeter voltage ranging from 1100 V to 100 nV and current range of 10.5 A to 1000 μA.

Figure 4.10.1 KEITLEY 2400 Source Measuring Unit

On the top of the deposited film 1cm x 1cm area is coated with Gold for electrode purpose. The Ito coated surface becomes one terminal and gold coat become the second terminal. By varying current or voltage the output voltage or current respectively can be calculated.

4.10.2 Four probe setup

Four probe set up is used to measure the Resistivity, Conductivity and Activation energy of thin films. By passing current through outer probes and measuring the voltage through inner probe and the resistivity of the thin film is calculated by using the formula.

$$\rho_0 = \frac{V}{I} \times 2\pi S \qquad \text{——————} \quad (4.4)$$

V – Voltage (V)

I – Current (A)

S – Spacing between the probes (0.2 cm)

The resistivity (ρ) of the thin film is given by

$$\rho = \frac{\rho_0}{G_7(W/S)} \qquad \text{(4.5)}$$

W – Film thickness

S – Distance between the probes

In our case $G_7(W/S)$ – 4.153

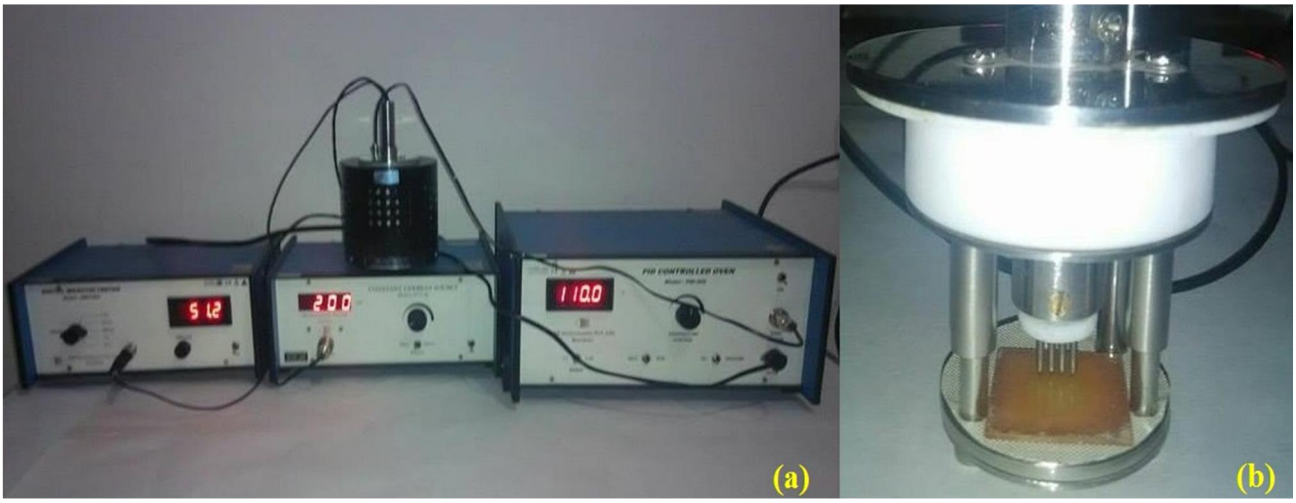

Figure 4.10.2 (a) Four probe setup used for resistivity measurement (b) thin film in the holder

The Energy Gap (E_g) is energy difference between highest point in valence (E_v) band and lowest point in the conduction band (E_c) and it is calculated by the formula.

$$\sigma = \sigma_0 \exp\left[-\frac{E_g}{2K_B T}\right] \qquad \text{(4.6)}$$

Where K_B – Boltzmann's constant, σ_o – Ideal conductivity of monocrystalline material,

σ – Electrical conductivity (S/cm)

Plot the ($\log_{10}\rho$) vs (1000/T) curves for the films and calculate the slope of that curves, which gives the value of E_g (eV).

4.10.3 Thin Film preparation for Electrical Characterization

Glass slides of 1" x 1" and 1 mm thickness were prepared for spin coating. One side of the slide was coated with ITO which is conducting side and the other side was non-conducting. On conducting side of the slides were coated with Fe doped ZnO sol by spin coating machine. 10 layers were deposited on conducting side of each slides and annealed at 500 °C and allowed for furnace cooling. Then on top of the coated surface 10 mm X 10 mm area was gold coated for electrode purpose and the bottom surface of the film was on the ITO coated surface (as shown in figure 10.12) which acts as second electrode. The electrode connections with KEITLEY 2400 Source Measuring Unit were made as shown in the figure. Voltage in the range of $\pm$ 10 mV was used as a source and output current in μA was measured and current in the range of $\pm$ 100 μA was used and output voltage in mV was measured. For both the cases V-I graphs were plotted. The Resistance (R) of the films was measured from these V-I plots.

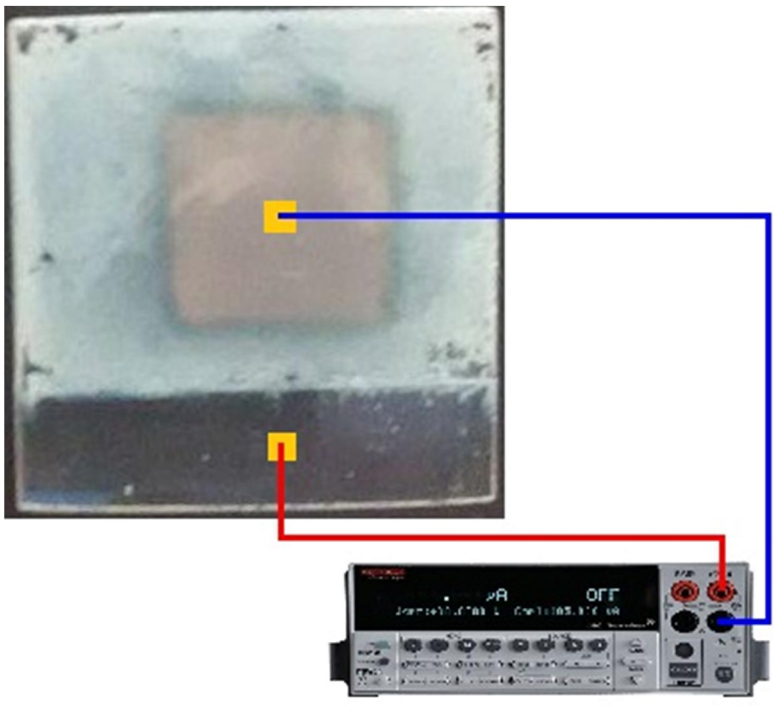

Figure 4.10.3 Schematic diagram of showing V-I measurements

5 RESULTS AND DISCUSSIONS

5.1 XRD Results

5.1.1 XRD analysis of Thin Film samples

All the thin film samples were analyzed by the Rigaku SmartLab XRD equipment. Initially two Fe doped ZnO thin films of $Zn_{(1-X)}Fe_XO$ (x=0.05) with molarity of 1M were deposited on glass wafer. The synthesized thin films were characterized by XRD (Cu Kα, λ= 1.5406 Å). Standard XRD diffraction peaks are (100), (002), (101), (102), (110), (103) and (112) located at 2θ = 31.548°, 34.163°. 36.036°, 47.372°, 56.391°, 62.814° and 67.819°. The films have preferred orientation along the (101). The samples did not show presence of any secondary phases (pure Fe, FeO, $ZnFe_2O_4$ and Fe_2O_3) indicating Fe has successfully substituted into ZnO lattice.

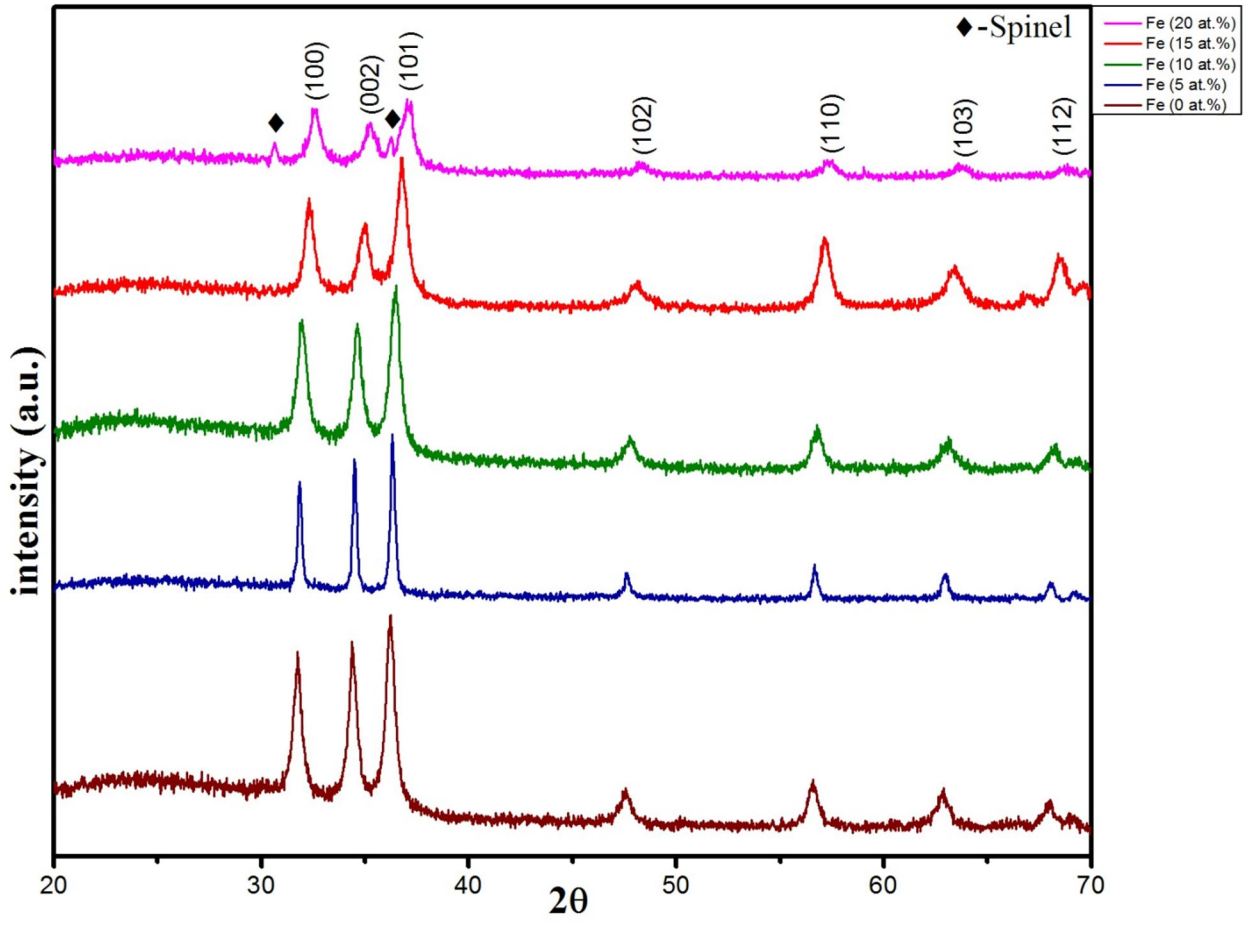

Figure 5.1.1 XRD patterns of Fe ($0 \leq X \leq 20$) doped ZnO thin films annealed at 500 °C

Then as shown in Figure 5.1.1 XRD pattern of $Zn_{(1-X)}Fe_XO$ ($0 \leq X \leq 20$) thin films were prepared by sol-gel and spin-coating method and all the films were grown on glass substrate. The films were annealed at temperature 500°C. All the thin film samples have a polycrystalline nature having diffraction peaks (100), (002), (101), (102), (110), (103) and (112). All the planes show (wurtzite) hexagonal crystal structure with a space group (P63mc) for the samples and are in good agreement with the ZnO (JCPDS 36-1451). The samples do not exhibits presence of any secondary phases like FeO, Fe_2O_3, Fe_3O_4 and Zn_2Fe_4O etc. This is may be due to small amount of impurities connot be detected in the XRD characterization. However for the sample $Zn_{0.80}Fe_{0.20}O$ we observe the presence of secondary phases like spinel ($ZnFe_2O_4$) (cubic crystal system) at $2\theta = 29.9415°$ and 35.3642°, small quantities of zincite, hematite (Fe_2O_3), magnetite (Fe_3O_4). As the Fe content increases we observe the decrease in intensity of all the diffracted peaks. The Fe can exist in both Fe^{2+} (0.78 Å) and Fe^{3+} (0.68 Å) valence states stably. As the ionic radius of Zn^{2+} (0.74 Å) which is smaller than Fe^{2+} (0.78 Å) and higher than Fe^{3+} (0.68 Å), there must be change in the peaks position. Also we analyzed the position of all the diffracted peaks and analysis suggest small shift towards higher 2θ angle. Hence it clearly show iron is present in Fe^{3+} valence state in our $Zn_{(1-X)}Fe_XO$ ($0 \leq X \leq 20$) thin film samples. Hence the crystal structure of ZnO is significantly affected by Fe doping concentration.

We have analyzed the results of structural changes as effect of Fe doping in ZnO such as lattice constant, average crystalline size and volume of unit cell. The peaks correspond to (002) and (101) directions tend to decrease as Fe content increases. This shows that ZnO lattice deformed because of the presence of increasing amount of Fe atoms in the Zn lattice as well as interstitial sites. We have also observed that in range of this Fe content the structural change is proportional to the incorporation of Fe atoms in samples. The variation of FWHM of (002) and (101) peaks gave a clear indication that average crystalline size of the samples has changed.

Lattice parameters (a and c), unit cell volume (V), lattice strain (ε) and average crystallite size (D) were calculated and the average crystallite sizes are approximately in the range of 11=18 nm and shown in the figure 5.1.2 and the values are tabulated in the table 5.1.1 and 5.1.2 XRD peaks of Fe doped ZnO films were broad compared to undoped ZnO indicating that the doping of Fe into the lattice of ZnO inhibited the crystallization of obtained samples. Fe^{3+} dopants resulted in lattice disorder and associated stresses. The lattice parameter (a) remains constant but lattice

parameter (c) decreases with the Fe content clearly indicates that Fe ions are substituting for Zn in the host ZnO lattice in a tetrahedral positions, as a result the unit cell volume decreases as Fe doping increases. This will induce the tensile stresses in the unit cell. This confirms Iron exist in 3+ state in our sample, as the large ionic radii of Zn^{2+} (0.74 Å) than Fe^{3+} (0.68 Å) [12] which causes distortion in the crystal lattice inducing more tension therefore affecting the growth of crystal. The difference in ionic radii of Zn^{2+} and Fe^{3+} in tetrahedral position is small, the change in the lattice parameter (c) and unit cell volume are also small with the increasing Fe concentration. Such decrease in lattice parameter due to TM dopeing have been observed by the sevaral authors [12], [23] and [25]

Average crystallite size for all the samples were calculated using Scherrer formula and (101) peak of the samples. The results show average crystallite size decreases with the increasing Fe doping concentration and the results were tabulated in the table 5.1.1. The results suggest that increase in doping prevents crystalline growth.

We do not observe any change in number of peaks therefore shift in 2θ is attributed to crystallite size modification in cations (Zn^{2+}). Also heating took place in presence of air this reduces the Oxygen vacancy but increases the Zn^{2+} vacancy therefore promotes the substitution of Fe^{3+} ions for Zn^{2+} sites.

Table 5.1.1 Average Crystallite size and lattice strain of Fe (0-20 at.%) doped ZnO Thin Films

Fe (at.%) in ZnO	Angle of (101) Peak	FWFM (Deg.) (101) peak	D (nm)	Lattice Strain ε (nm)
0	36.1959	0.480	18.187	0.0064
5	36.2257	0.488	17.90	0.0065
10	36.3367	0.528	16.55	0.0070
15	36.3723	0.576	15.169	0.0077
20	36.4741	0.768	11.379	0.0102

The lattice parameters (a and c) of hexagonal wurtzite unit cell of Fe doped ZnO thin films has been calculated by using the lattice spacing (*d*) and (*hkl*) values. For hexagonal wurtzite type of crystal systems the *a* and *c* were calculated by using Bagg's law and the follwing relations. [12]

$$\frac{1}{d^2} = \frac{4}{3}\left(\frac{h^2+hk+k^2}{a^2}\right) + \frac{l^2}{c^2} \qquad \text{——— (5.1)}$$

$$\frac{4\sin^2\theta}{\lambda^2} = \frac{4}{3}\left(\frac{h^2+hk+k^2}{a^2}\right) + \frac{l^2}{c^2} \qquad \text{——— (5.2)}$$

d – lattice spacing (nm), which was also determined from the SAED pattern

h,k,l – Miller indices

θ – angle of the corresponding peak

λ – waveleght of radiation used Cu K_α (1.5406 Å)

In the above formula two (a and c) unknowns are there, so for the calculation of lattice constant a, we have cocnsidered the peak (h00) or (hk0) for example (100) to eliminate the c. In the same way for the calculation of lattice parameter c the peak in the form (00k) like (002) was choosen in order to reduce the equation with any one unknown.

Table 5.1.2 Lattice parameter and Volume of unit cell of Fe (0-20 at.%) doped ZnO thin films

Fe (at.%) in ZnO	a (Å)	c (Å)	Zn-O Bond Length L_c (Å)	Volume of Unit Cell ($nm^3\ 10^{-3}$)
0	3.2535	5.2151	1.9804	47.806
5	3.2480	5.2083	1.9772	47.507
10	3.2531	5.2048	1.9761	47.306
15	3.2417	5.1876	1.9721	47.211
20	3.2422	5.1760	1.9709	47.120

Volume of the wurtzite hexagonal unit cell of $Zn_{(1-X)}Fe_XO$ ($0 \leq X \leq 20$)is given by [12]

$$\mathbf{V = a^2 c \sin 60°} \quad \text{———} \quad (5.3)$$

Where a, c – are lattice parameters

It is important to note that the substitution of foreign Fe ions in host ZnO lattice has caused remarkable change in the Zn – O bond length. For hexagonal crystal system the bond length (L) is calculated by the formula. The value of *u* (Positional parameter) is given by. [29]

$$L = \sqrt{\left(\frac{a^2}{3} + \left(\frac{1}{2} - u\right)^2 c^2\right)} \quad ; \quad u = \frac{a^2}{3c^2} + 0.25 \quad \text{———} \quad (5.4)$$

The values of variation of bond length (L) with the Fe doping content is tabulated in the table 5.1.2. For pure ZnO the Zn – O bond length is 1.9804 Å. The values of Zn – O bond length was found to be increasing with the increasing Fe doped ZnO samples this is because of incorporation of Fe ions in the host ZnO lattice.

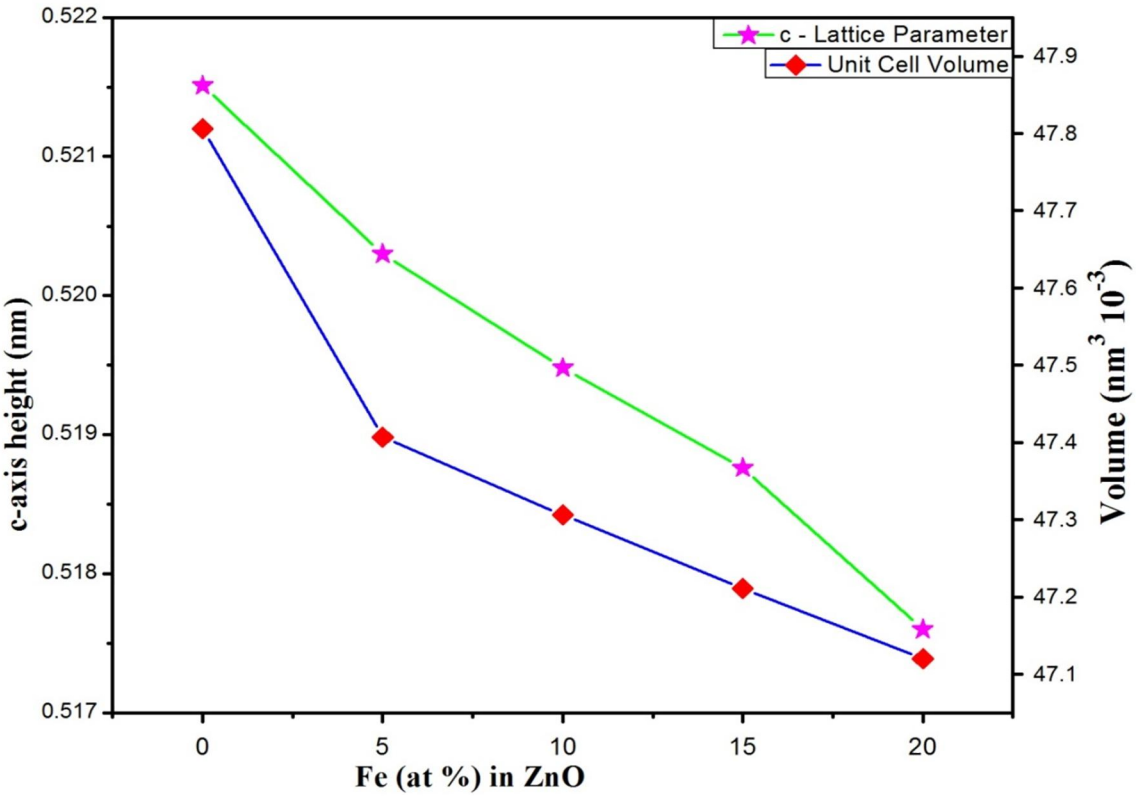

Figure 5.1.2 Variation of c-axis height and Unit cell volume vs Fe (at.%) in ZnO thin films

5.1.2 XRD analysis of powder samples

We have also prepared powder of ZnO doped with Fe (0 – 20 at.%) for the analysis of SQUID and HRTEM, all the samples show similar characteristics of the corresponding thin film samples. However the peak intensities of all the samples were higher that the corresponding thin films coated on glass substrate. This is because of amorphous nature of the glass substrate. All the samples have a polycrystalline nature. The diffraction peaks (ZnO) are (100), (002), (101), (102), (110), (103) (200) (112) and (201) and located at an angle 2θ = 31.6313°, 34.1251°. 36.1512°, 47.4216°, 56.4711°, 62.7584°, 66.3024°, 67.986° and 69.0425° respectively. For Fe (20 at.%) doping concentration spinel ($ZnFe_2O_4$) phase at 2θ = 29.8462° and 35.2618° appears, this suggest that the solubility of Fe in ZnO is limited up to 20 at.%.

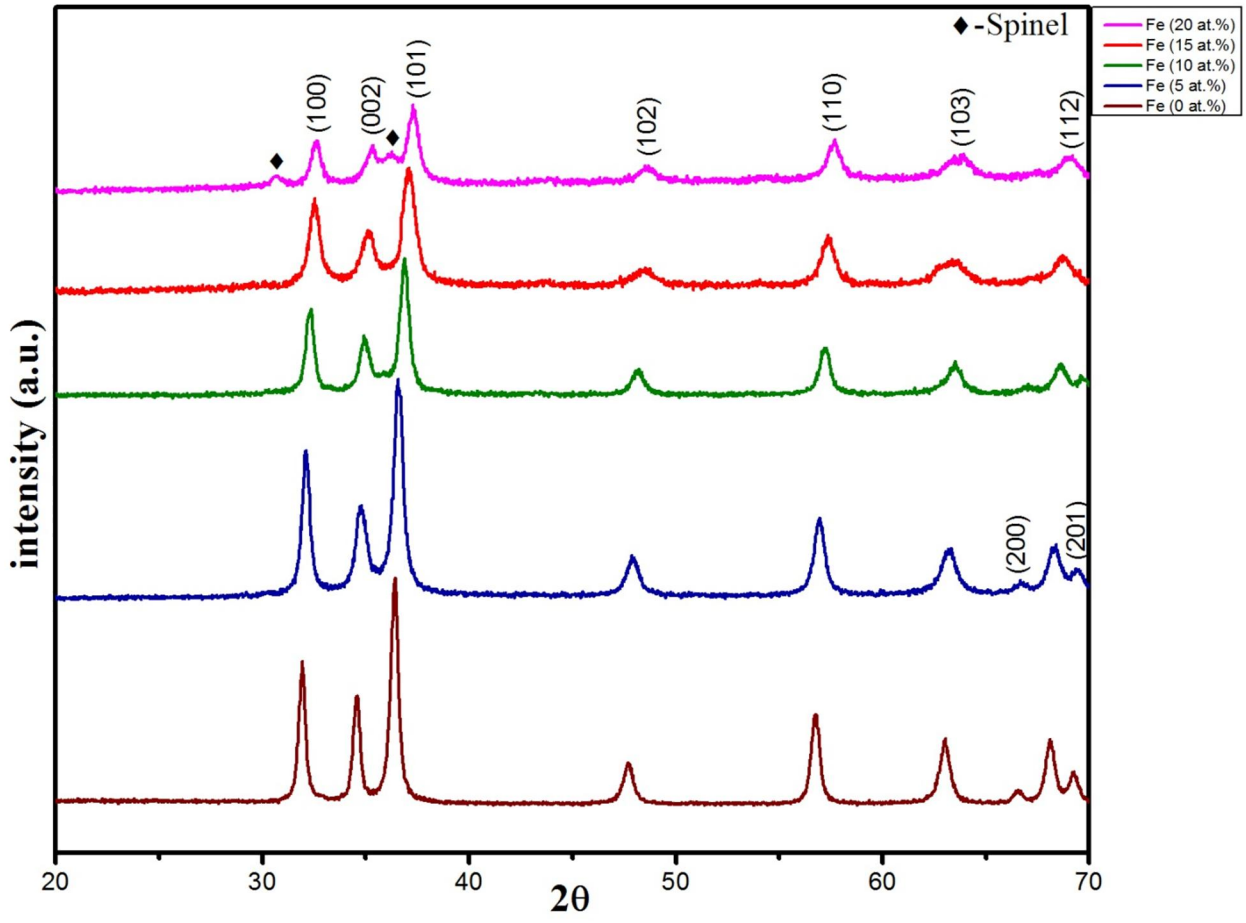

Figure 5.1.3 XRD patterns of Fe doped ZnO Powder samples annealed at 500 °C

5.1.3 XRD analysis of Fe (10 at.%) doped ZnO Powder annealed at different temperatures

The powder sample of $Zn_{0.90}Fe_{0.10}O$ was synthesised in the same manner as the above samples. The four samples were taken exactly the same weight and subjected to annealing at 400 °C, 500 °C, 600 °C and 700 °C in the presence of air for 2 hours and allowed them for furnace cooling. Figure 5.1.4 shows XRD pattern of Fe 10 at.% in ZnO at different annealing temperatures.

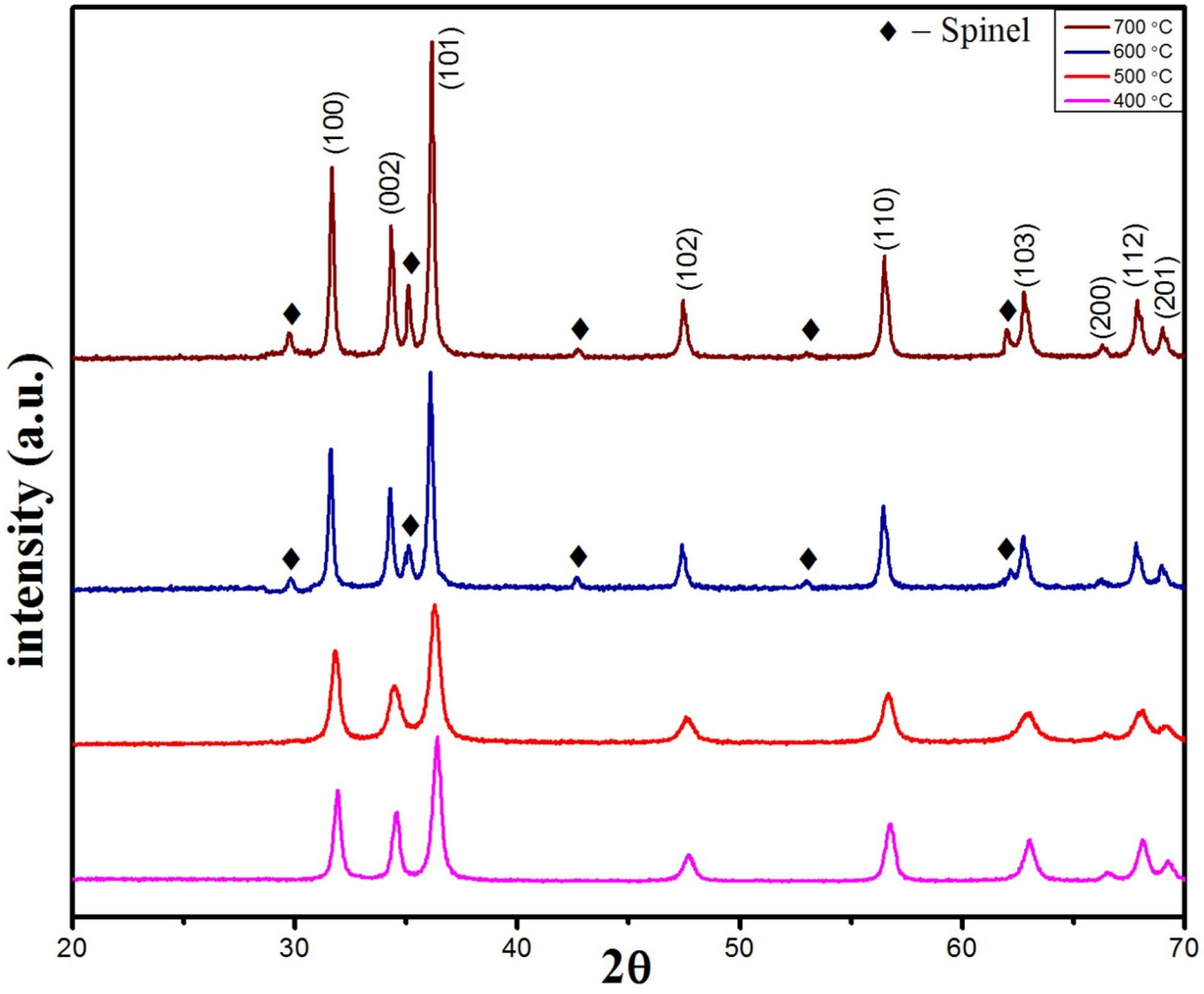

Figure 5.1.4 XRD patterns of Fe (10 at.%) doped ZnO powder at different annealing temperatures

The results show as the annealing temperature the intensity of the peaks increases because of very slow cooling rate the internal stresses are relieved, peaks at higher temperature are sharper than the lower ones implying crystallite size has increased. This is due to grains grow larger as

the annealing temperature increases. Also we did not observed any considerable changes in the peak positions. Figure 5.1.5 shows variation of average grain size with annealing temperature. Also as annealing temperature increases above 500 °C i.e. at 600 °C and 700 °C spinel and other secondary phases were appeared which restrict us annealing temperature of $Zn_{(1-X)}Fe_XO$ ($0 \leq X \leq 20$) samples at 500 °C.

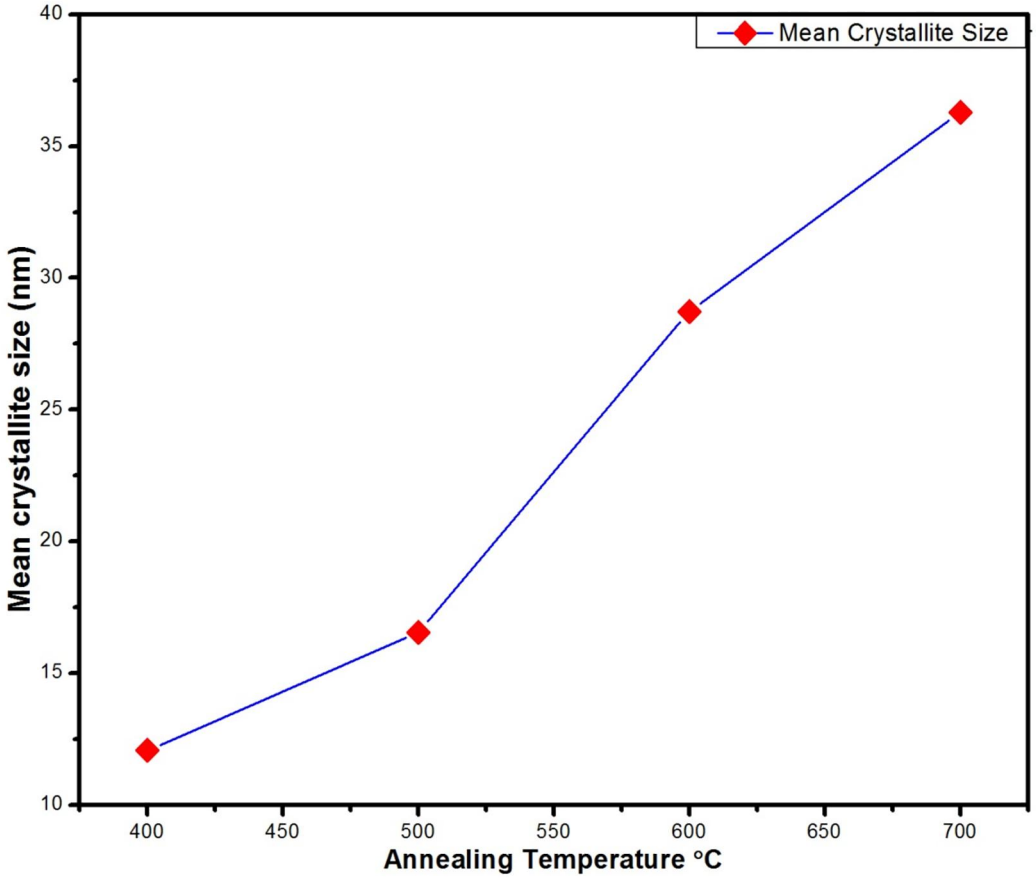

Figure 5.1.5 Variation of Mean crystallite size with Annealing temperature

The average crystallite sizes of the samples were calculated using Scherer equation.

$$D = \frac{0.9\lambda}{\beta \cos\theta} nm \quad \text{——} \quad (5.5)$$

Where D = Mean crystallite size

λ = WL of X-ray used (1.5402 Å)

β = FWHM of the most intense peak

5.2 FE-SEM and EDX Results of Fe (0-20 at.%) doped ZnO Thin Films

5.2.1 FE-SEM analysis of Thin films

FE-SEM (Carl Zeiss Ultra Plus) was used to study the morphology of the $Zn_{(1-x)}Fe_xO$ ($0 \leq X \leq 20$) thin films deposited on glass substrate annealed at 500 ˚C in air. Figures show the FE- SEM images of the Fe doped ZnO thin film by Sol-gel method. The films obtained are uniform and have a homogeneous surface distribution of particles. Also Fe particles are uniform throughout the film surface and the particles are in spherical shape and are in the range of 27 nm to 50 nm. The particle size of the films depends on the Fe concentration in ZnO solution and thickness of the layer. We can see from the figure 5.2.1 to figure 5.2.5 with the increases in Fe concentration the particle size decreases. This may be due to fact that as Fe content increases Fe ions not only substitute the Zn vacant sites but also occupies the interstitial sites. Which obstruct the crystal growth this distortion produced by the Fe atoms inside the ZnO lattice is responsible for the reduction in particle size and this is in good agreement with the other authors also [22 – 25].

5.2.2 EDX measurements

EDX (Energy dispersive X-ray spectroscopy) analysis was carried out to determine elemental compositions of the thin film samples. Inset of figures 5.2.1 – figure 5.2.5 show EDX analysis of ZnO thin film samples for Fe (0-20 at.%) The EDX images show Zn, O and Fe elements and no traces of other elements were found in the EDX spectra confirming the purity of ZnO thin film samples. Inset of each figure shows peak intensity of Zn, Fe and O. The EDX spectrum clearly shows peak intensity (Fe Kα) of Fe increase as its concentration increases in ZnO. This also verifies the estimated elemental composition of the thin films for $Zn_{(1-x)}Fe_xO$ ($0 \leq X \leq 20$), the results are tabulated in the table 5.2.1 – table 5.2.5.We can see in each table difference in the composition values of Zn and O (at.%) column, even though they are in the ratio 1:1. However, the exact chemical composition of the films could not be obtained with 0 % Error. This may be due to presence of Oxygen in the glass substrate, atomic number and absorption co-efficient of the elements present and the substrate.

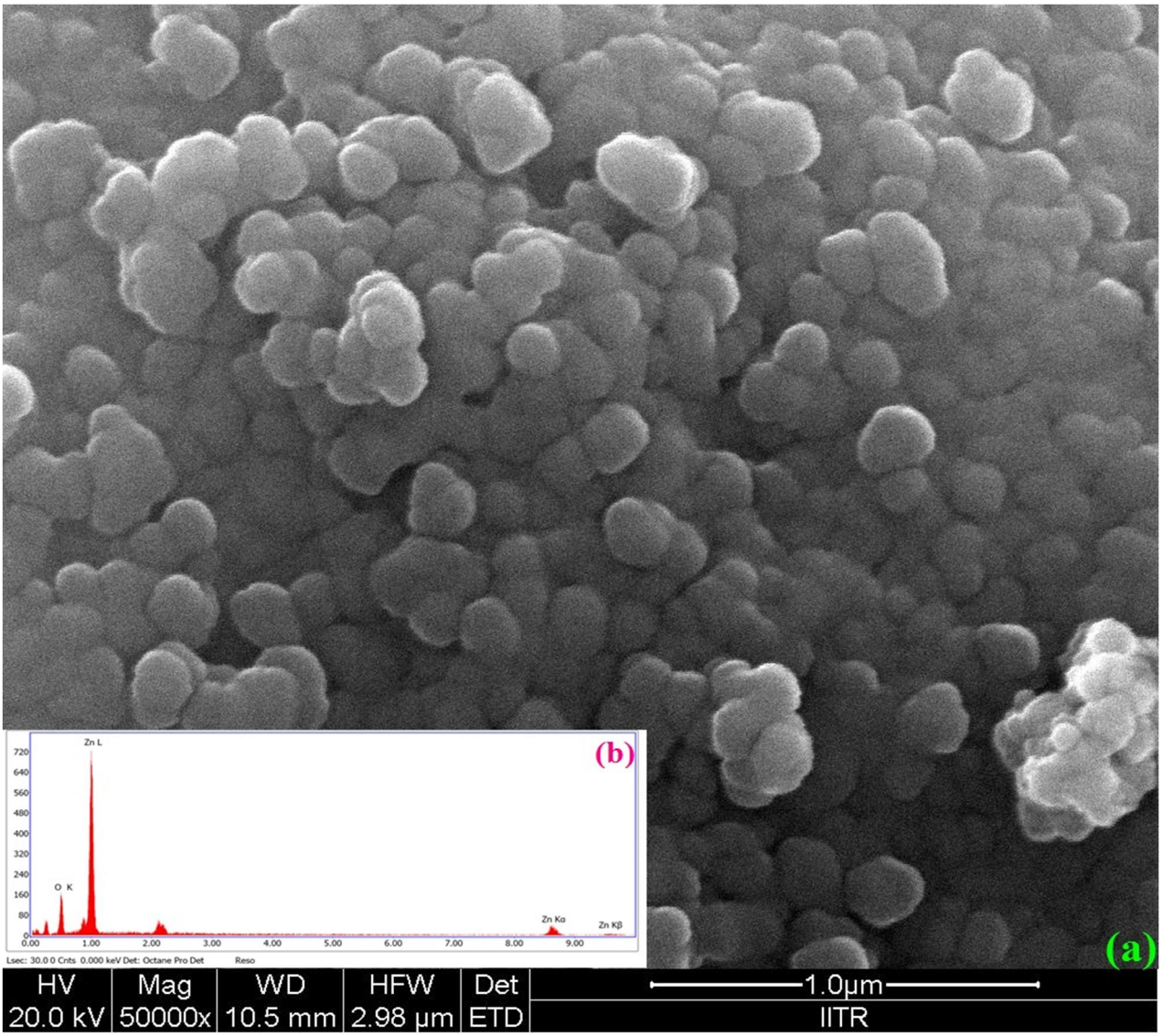

Figure 5.2.1 (a) FE-SEM image of ZnO and (b) its EDX spectrum

Table 5.2.1 EDX analysis of Elemental composition of ZnO thin film

Element	Weight %	Atomic %	Net Int.	Error %
O K	23.86	56.15	65.15	10.44
Zn K	76.14	43.85	114.89	4.89

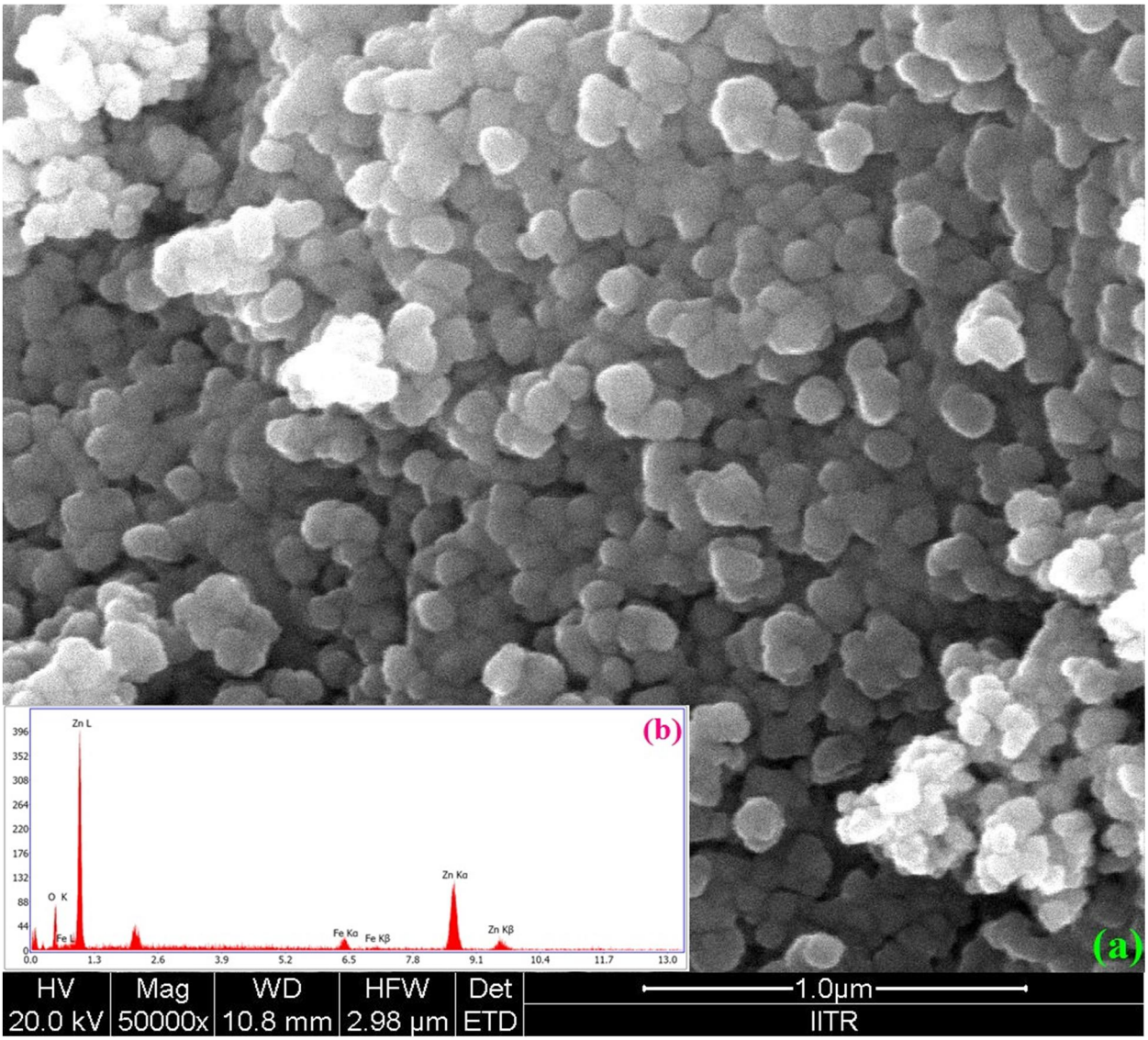

Figure 5.2.2 (a) FE-SEM image of $Zn_{0.95}Fe_{0.05}O$ and (b) its EDX spectrum

Table 5.2.2 EDX analysis of Elemental composition of $Zn_{0.95}Fe_{0.05}O$ thin film

Element	Weight %	Atomic %	Net Int.	Error %
O K	15.07	41.78	43.41	10.77
Fe K	5.26	4.18	22.13	5.08
Zn K	79.67	54.05	133.78	3.13

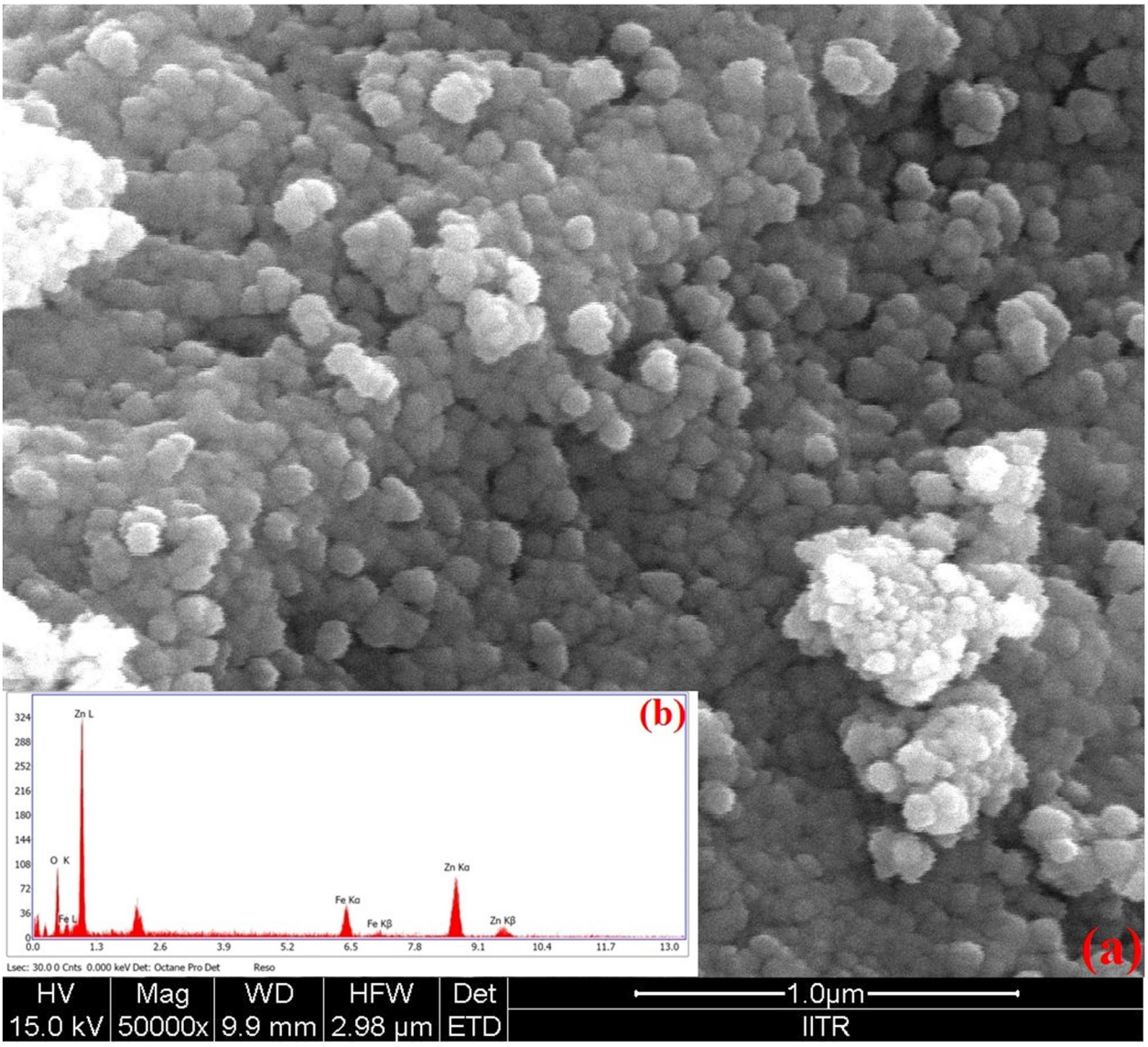

Figure 5.2.3 (a) FE-SEM image of $Zn_{0.90}Fe_{0.10}O$ and (b) its EDX spectrum

Table 5.2.3 EDX analysis of Elemental composition of $Zn_{0.90}Fe_{0.10}O$ thin film

Element	Weight %	Atomic %	Net Int.	Error %
O K	17.57	45.9	37.00	0.03
Fe K	12.99	9.72	35.70	0.09
Zn K	69.43	44.38	79.50	0.03

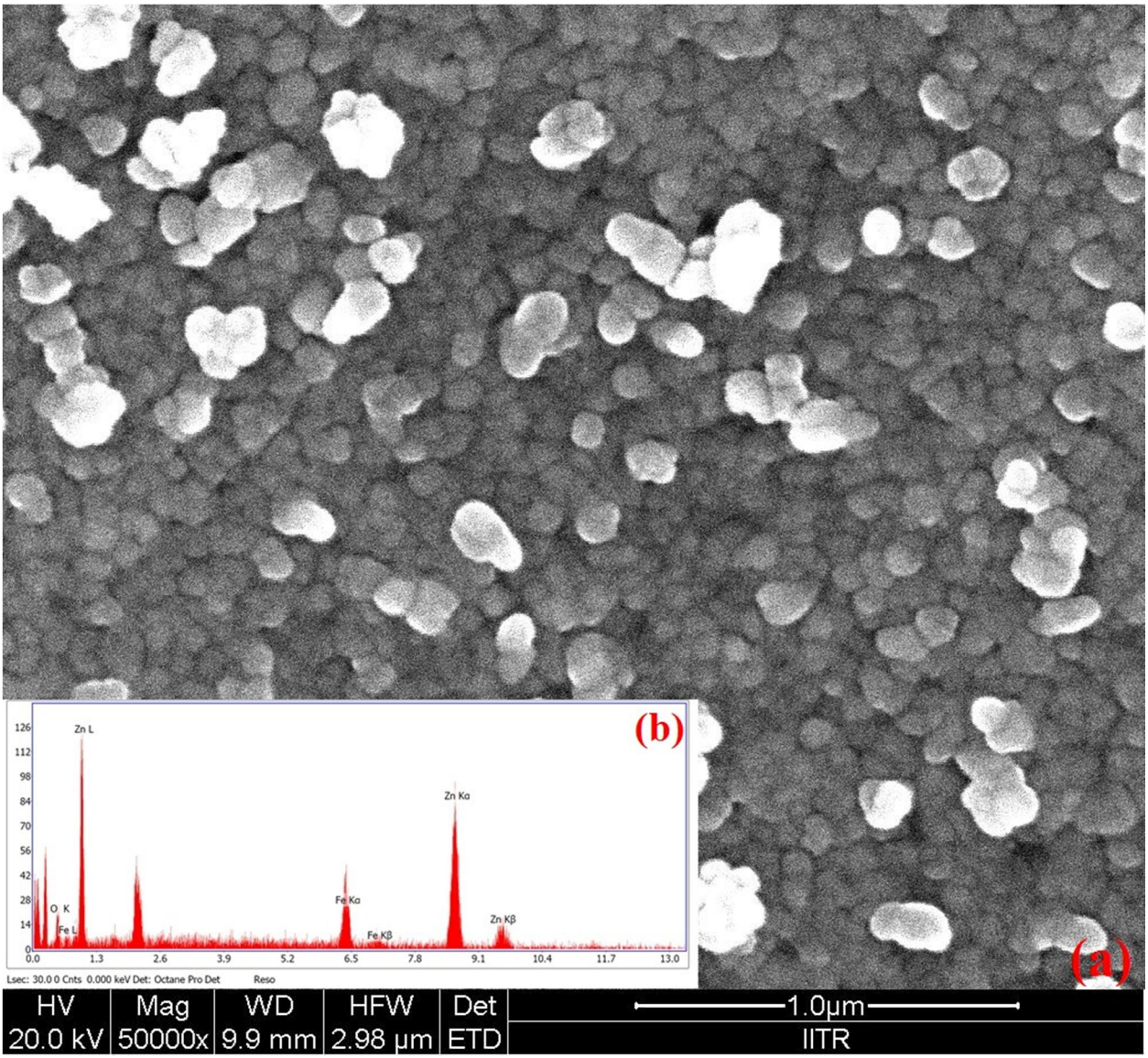

Figure 5.2.4 (a) FE-SEM image of $Zn_{0.85}Fe_{0.15}O$ and (b) its EDX spectrum

Table 5.2.4 EDX analysis of Elemental composition of $Zn_{0.85}Fe_{0.15}O$ thin film

Element	Weight %	Atomic %	Net Int.	Error %
O K	3.63	13.06	5.77	23.60
Fe K	14.29	14.72	33.81	11.75
Zn K	82.07	72.22	80.22	5.34

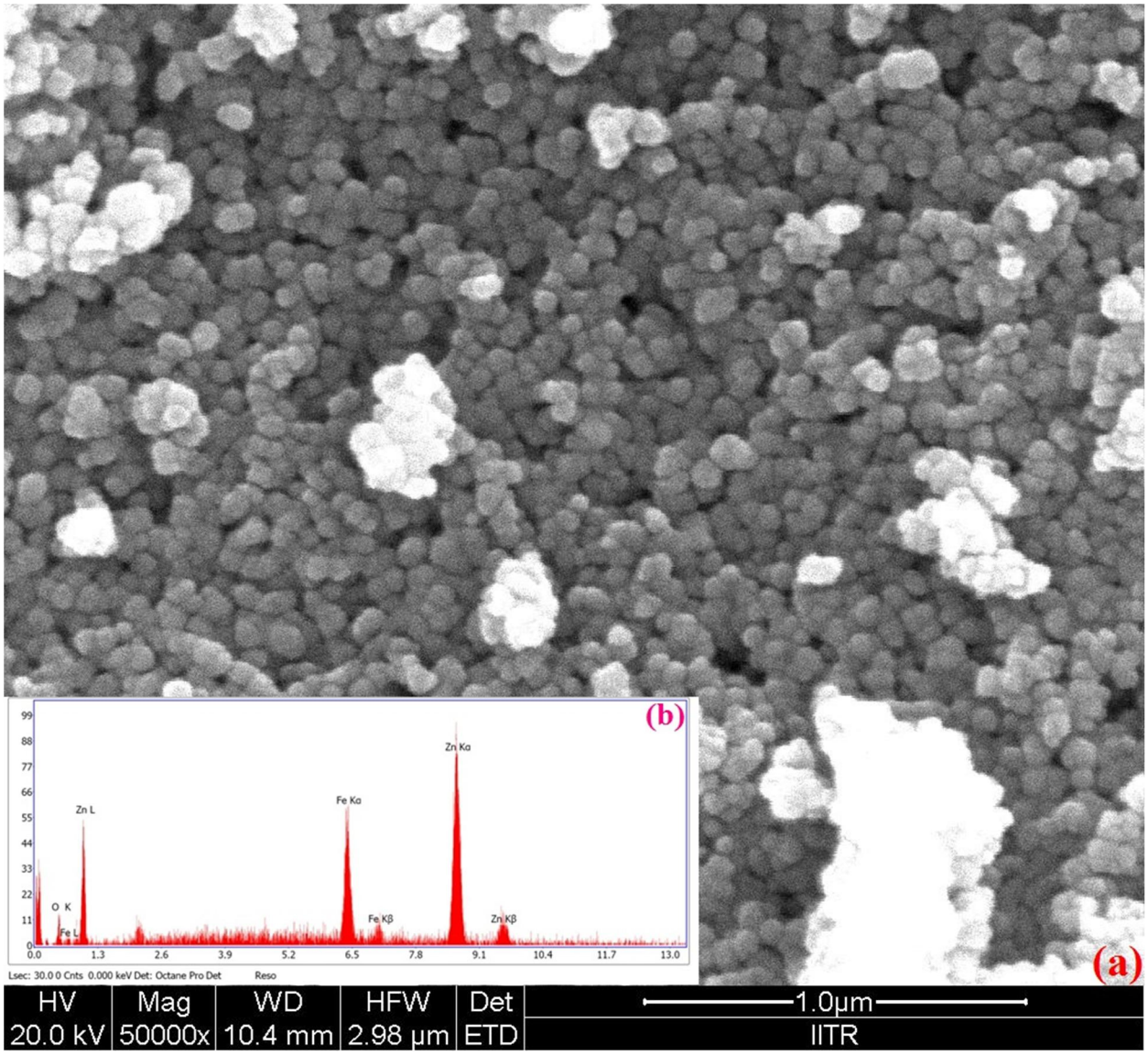

Figure 5.2.5 (a) FE-SEM image of $Zn_{0.80}Fe_{0.20}O$ and (b) its EDX spectrum

Table 5.2.5 EDX analysis of Elemental composition of $Zn_{0.80}Fe_{0.20}O$ thin film

Element	Weight %	Atomic %	Net Int.	Error %
O K	2.17	8.05	4.29	21.64
Fe K	20.09	21.36	56.89	4.89
Zn K	77.74	70.59	92.80	4.17

Table 5.2.6 Variation of Average particle size of Fe (0-20 at.%) doped ZnO thin films annealed at 500 ºC temperature

Fe (at.%) in ZnO	No. of Particles	Avg. Area (nm^2)	Avg. Diameter (nm)
0	102	1917.368	49.4092
5	114	1449.541	42.9606
10	122	1123.069	37.8145
15	129	778.525	31.4841
20	136	603.817	27.7273

Table 5.2.7 Variation of Average particle size of Fe (10 at.%) doped ZnO thin films annealed at different temperatures

Annealing Temperature (ºC)	No. of Particles	Avg. Area (nm^2)	Avg. Diameter (nm)
400	97	640.952	28.5672
500	65	1060.135	36.7397
600	49	1574.722	44.7772
700	36	2605.328	57.5952

For measuring the average particles size we have used the IMAGEJ software. The table 5.2.6 show the average particles size of the thin films for Fe (0-20 at.%). From the table we can see that as Fe concentration in ZnO increases the number of particles per unit area increases i.e. particles become smaller. This is due to incorporation of impurity (Fe) ions in the host (ZnO) lattice sites (also at the interstitial sites), ionic radius of Fe being smaller that Zn resulting stresses (tensile) and distortion in the host lattice. This restricts the growth of particles and affecting the crystal structure of ZnO significantly because of Fe dopant.

5.2.3 Fe (10 at.%) doped ZnO thin films at different annealing temperatures

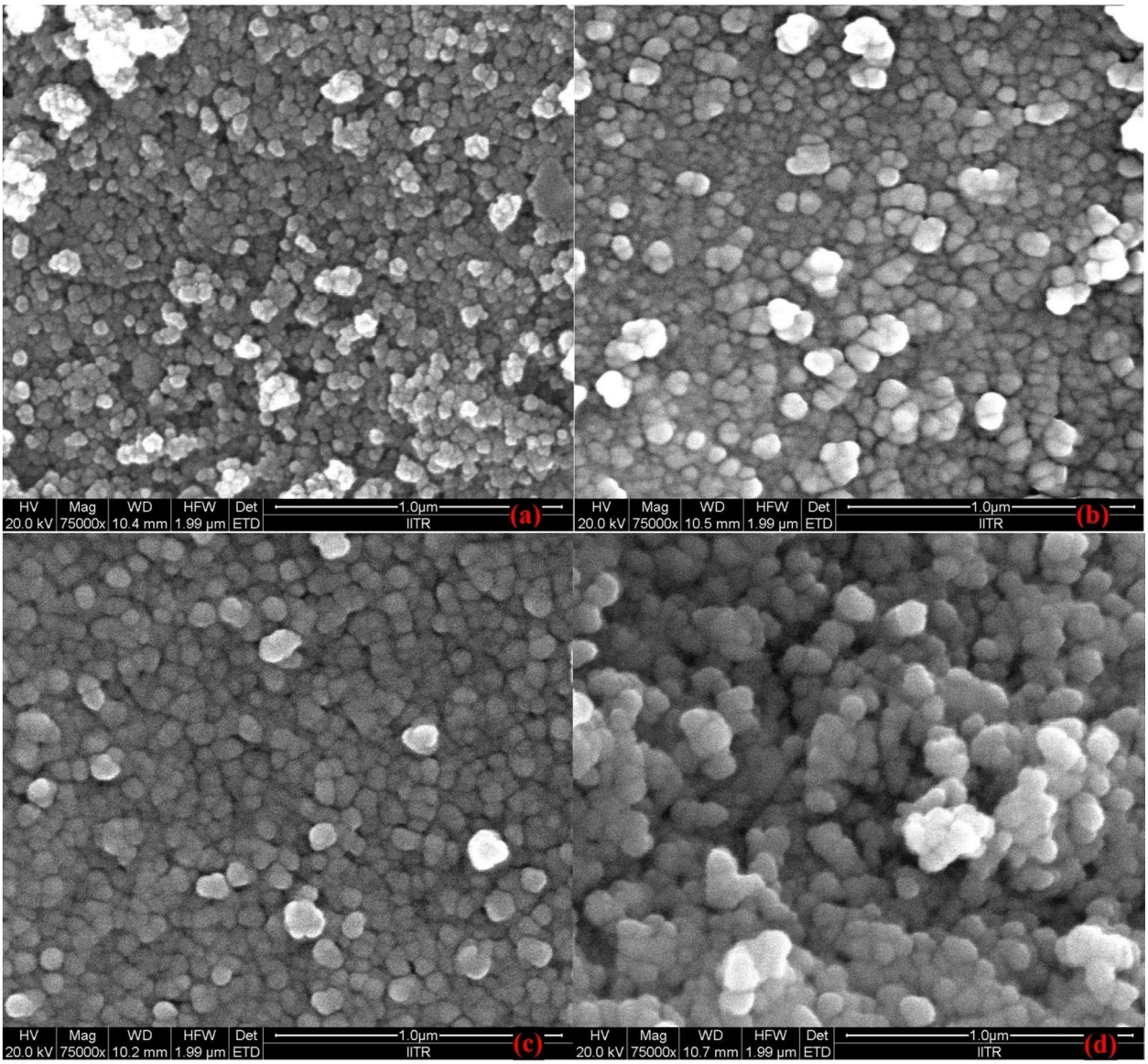

Figure 5.2.6 FE-SEM images of $Zn_{0.90}Fe_{0.10}O$ thin films annealed at (a) 400 °C (b) 500 °C (c) 600 °C (d) 700 °C

We studied the affect of annealing temperature on the size of the particles and morphology of thin films for $Zn_{0.90}Fe_{0.10}O$. We have prepared four $Zn_{0.90}Fe_{0.10}O$ thin films which were annealed in presence of atmospheric air in a furnace at different temperatures (400, 500, 600, 700 °C) for 2 hours and allowed them for furnace cooling. Then the morphology of thin films was analyzed by FE-SEM and the shown in the figure 5.2.6. We have analyzed the variation of average particle

size with the annealing temperature. The results are tabulated in the table 5.2.7 and we can see that increasing the annealing temperature of the thin films particles grow larger. However at higher annealing temperature (> 500 °C) the risk of secondary phases formation is higher, some of them are not desirable for electrical and magnetic properties of films.

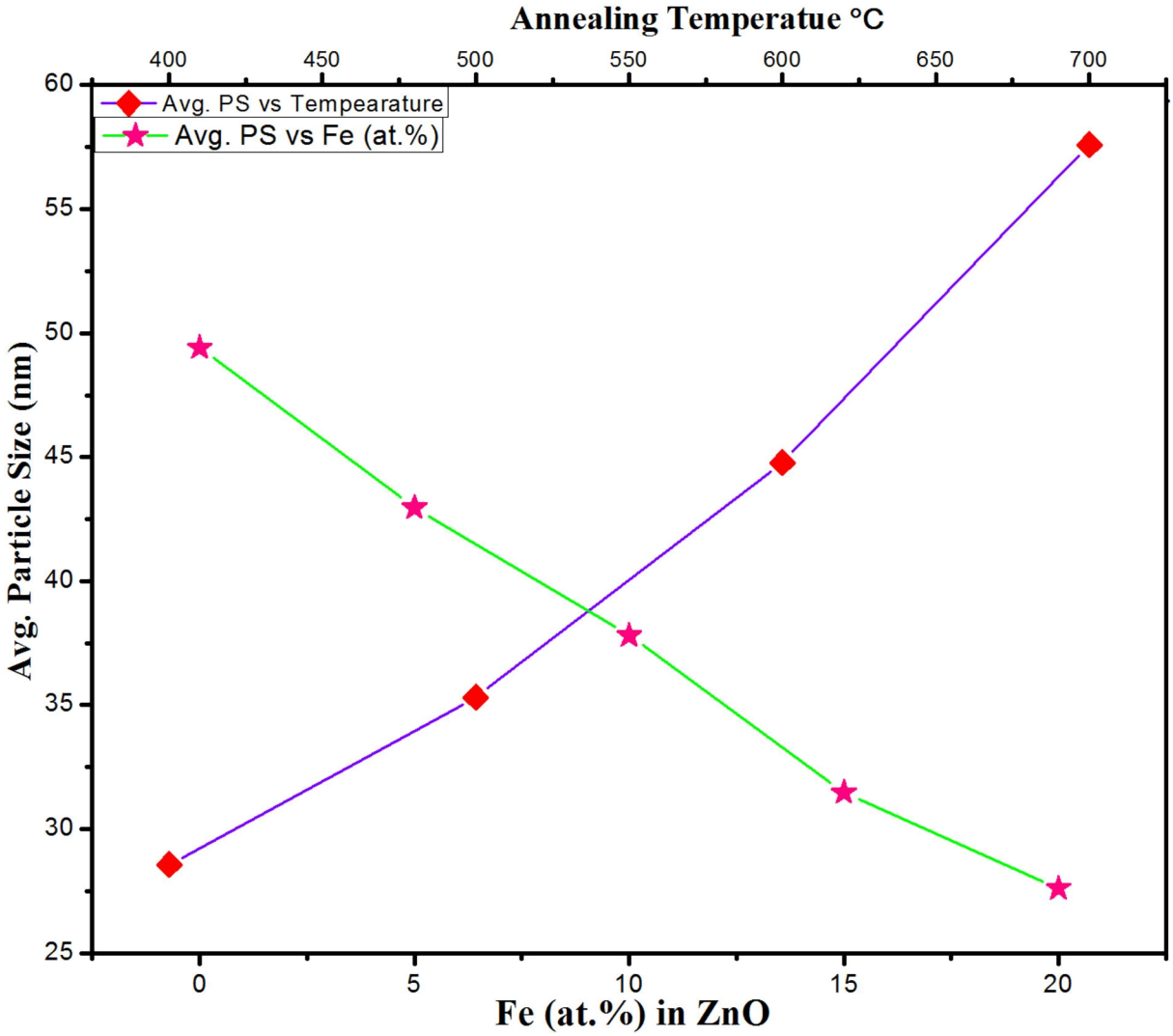

Figure 5.2.7 Average Particle size vs Fe (at.%) and Annealing Temperature

The average particle size was calculated using the Imagej software. We have selected the particles randomly and the diameter of each particle has been measured in three different directions, like this we have selected number of particles and average has been calculated for each Fe doping concentration (0 – 20 at.%) and the values are tabulated in the table 5.2.6. The particle size ranges approximately from 27 nm to 49 nm. We can see as the Fe dopant increases in the ZnO particle size decreases consistently.

5.2.4 EDX – Mapping of Fe (10 at.%) doped ZnO thin film

EDX – mapping is an element map of image showing the spatial (scattering) distribution of elements in the test sample. It is a 2 – dimensional section of the test specimens, which are very useful for revealing distribution of elements in the samples in visual and physical quality of a surface (textural) especially for showing compositional regions. This helps in determining the different phases present over the selected area and give 2-D image of internal chemical zonation surrounding or within an alloy or mineral (organic or inorganic).

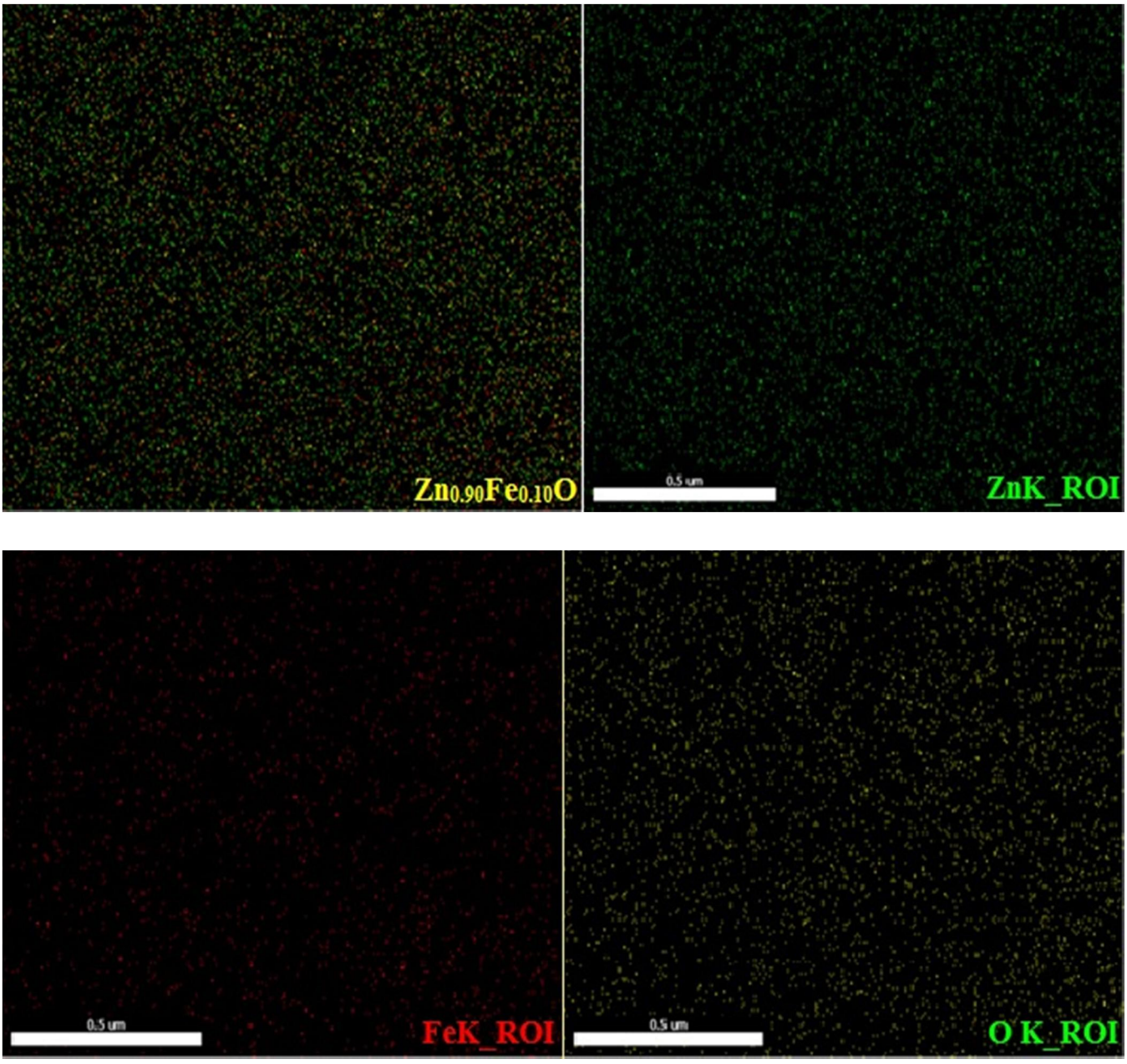

Figure 5.2.8 EDX – Mapping of $Zn_{0.90}Fe_{0.10}O$ thin film synthesised by Sol-gel method

5.3 Scanning Probe Microscopy (SPM) analysis of thin films

SPM (NT-MDT-INTEGRA) is used to analyze the structural and topographical characterization technique for the analysis of thin films in contact mode. Roughness of the thin films was analyzed by the SPM. Figure 5.3.1 – figure 5.3.5. Show the 3-dimensional surface morphology of ZnO thin films doped with Fe and deposited on glass substrate. The selected scan area was 10μm X 10μm from the figures we can see that all the films have dense and uniform ZnO/Fe grains. The shape of the grains is columnar shape (pyramidal) and they grow preferentially along the c-axis that is perpendicular to the glass substrate surface. These results are in excellent agreement with the XRD results. For the samples as Fe doping concentration increases their grains tends to decrease. This is due to large strain induced in the films which affects the normal growth of ZnO grains.

As we have seen from FE-SEM analysis as the Fe dopant increases in the ZnO the particle size decreases. The inset of each figure shows the scanned area of the thin film. Figure 5.3.6 show the graph of Fe doping concentration vs Average surface roughness. From the graph and table 5.3.1 we can see that for pure ZnO film has more surface roughness, but as Fe dopant increases in the ZnO surface roughness gradually decreases. This could be connected with decrease of ZnO grains as Fe concentration increases in the films. The similar results are also reported by Chen et al. [26] and Wang et al [27]

The surface roughness are expressed in in terms of Average Roughness (Ra) and Root Mean Square (RMS) (Rq) given by the formulae.

$$Ra = \frac{1}{L}\int_0^L |z(x)|dx \;\; ; \;\; R_q = \sqrt{\frac{1}{L}\int_0^L z^2(x)\,dx} \qquad \text{——— (5.6)}$$

Ra – is the arithmetic average of the absolute values of the surface or profile height deviations measured w.r.t. mean line. It is in microns

RMS – is the (geometric average height) square root of the average of the roughness profile height deviations measured within the sample length w.r.t. mean line and is more sensitive to peaks and valleys. RMS is recorded in micro-inches.

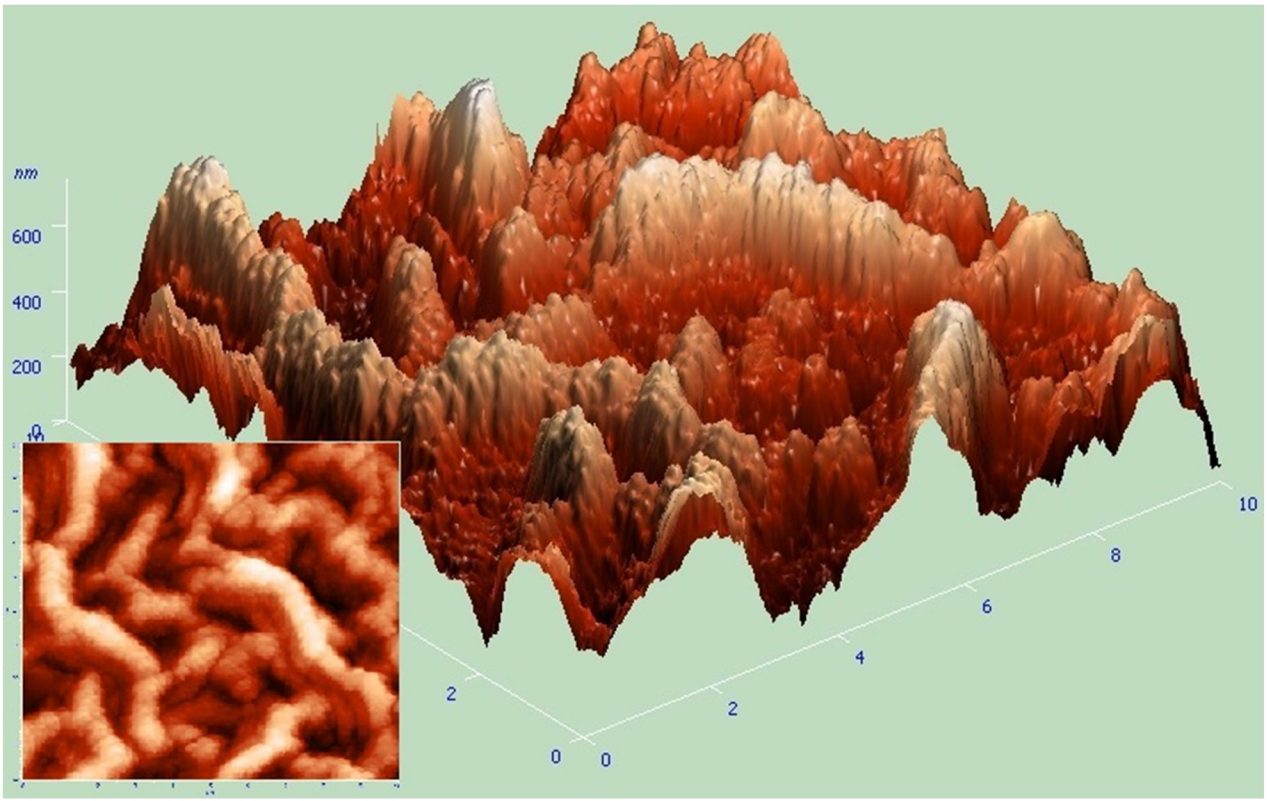

Figure 5.3.1 Surface morphology image of ZnO thin film

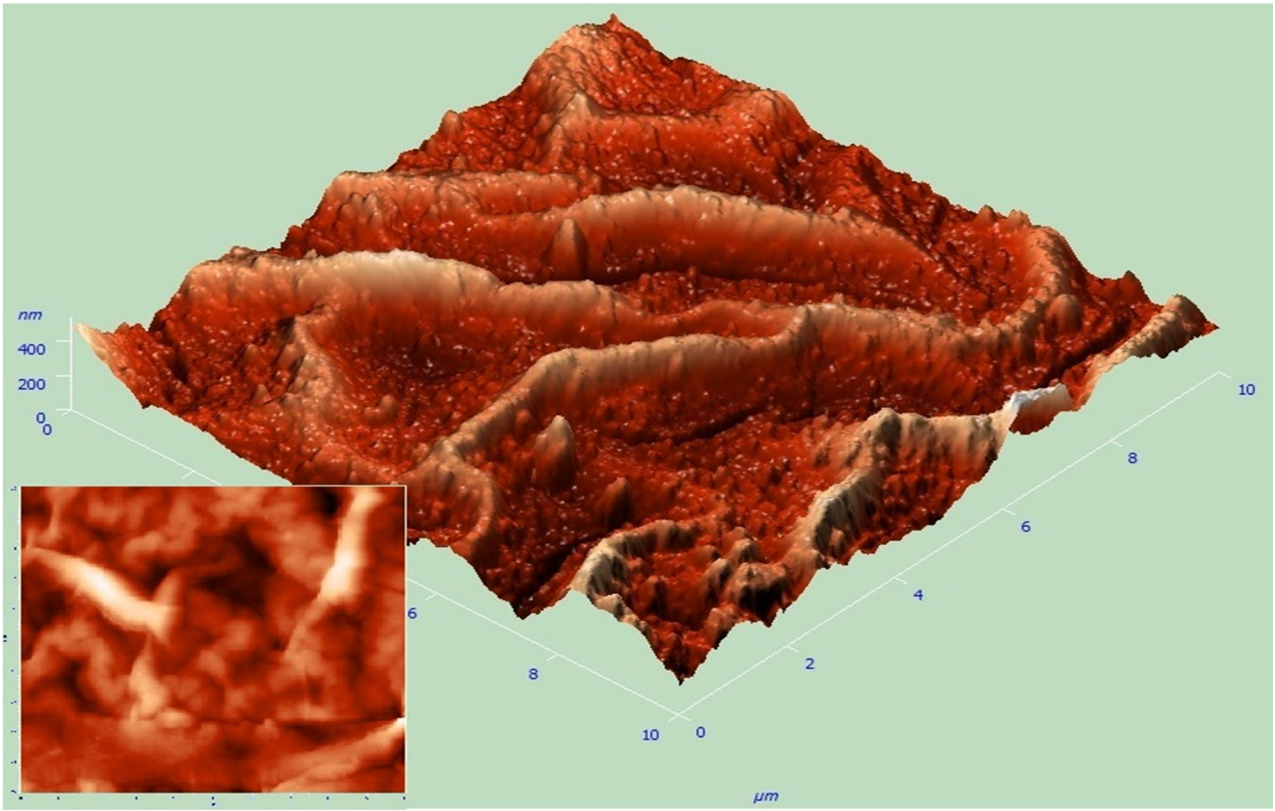

Figure 5.3.2 Surface morphology image of $Zn_{0.95}Fe_{0.05}O$ thin film

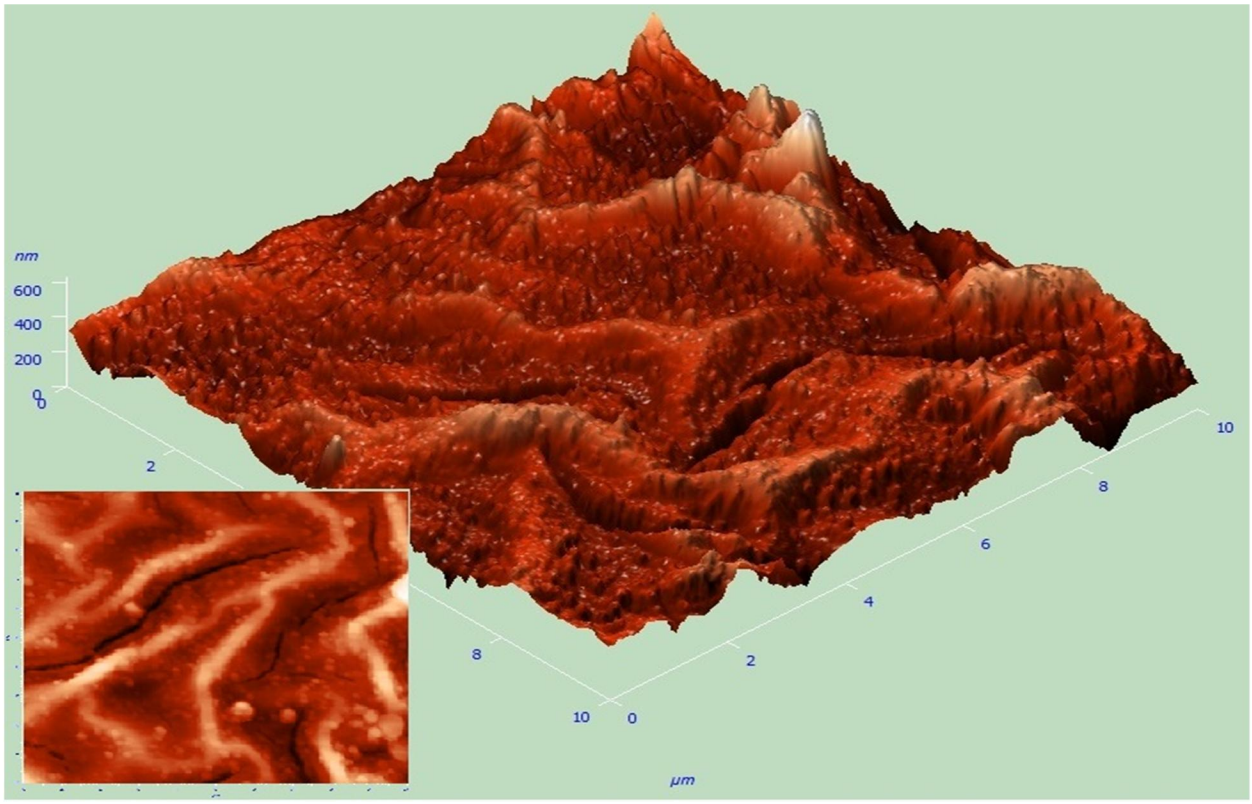

Figure 5.3.3 Surface morphology image of $Zn_{0.90}Fe_{0.10}O$ thin film

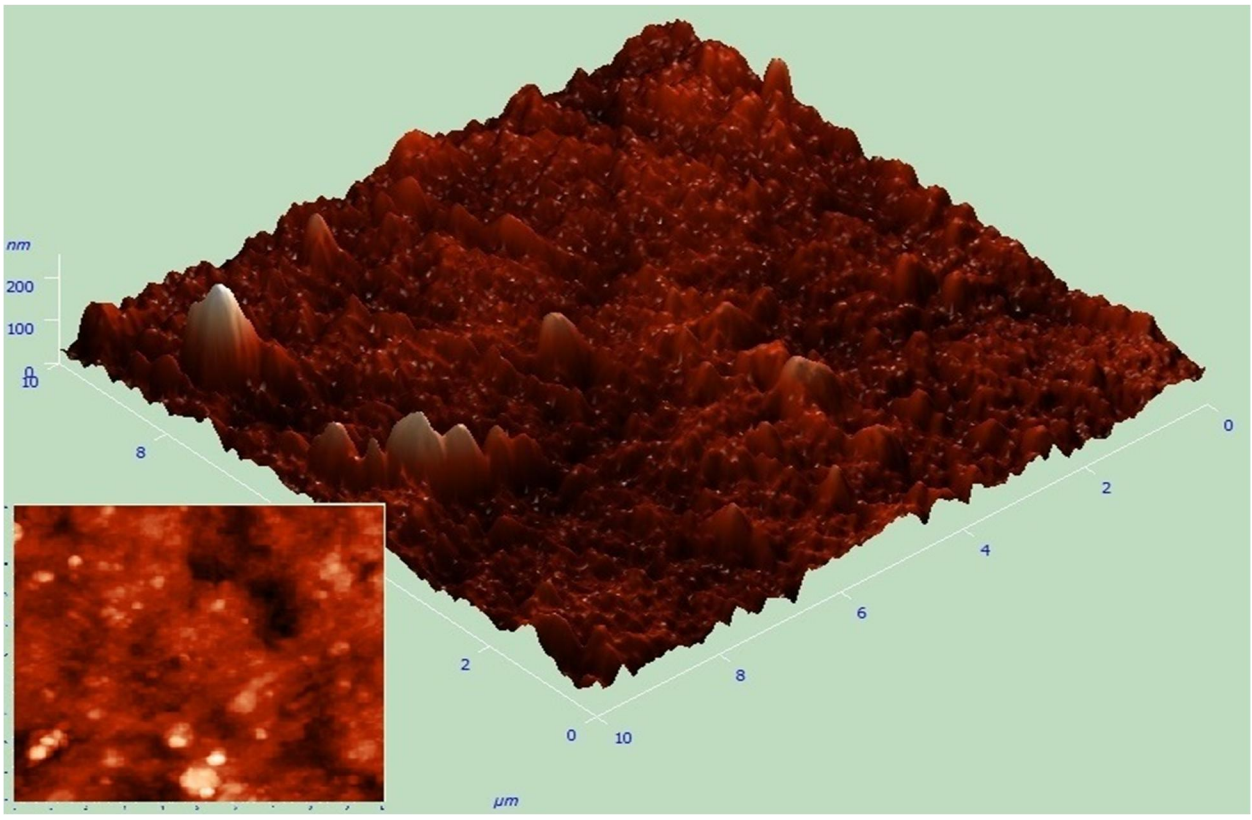

Figure 5.3.4 Surface morphology image of $Zn_{0.85}Fe_{0.15}O$ thin film

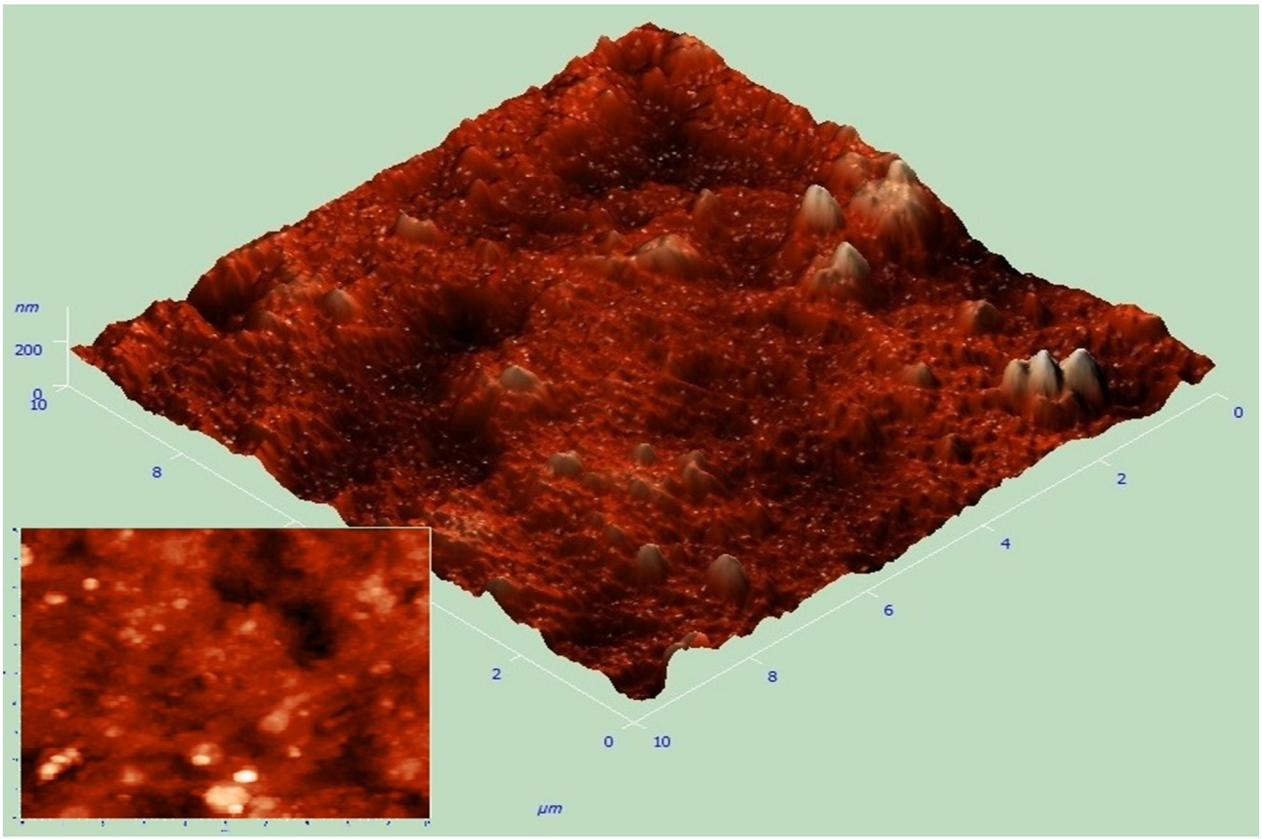

Figure 5.3.5 Surface morphology image of $Zn_{0.80}Fe_{0.20}O$ thin film

The main difference between the Ra and RMS scales is that single large peak or valley in the surface texture will considerably raise the Rq value. For a given microscopic surface profile, therefore, the value of Rq will be higher than the Ra value; generally RMS is accepted 11% higher than the Ra value. Also Ra measurement values do not gives the true picture of the microscopic surface.

Conversion of Ra to RMS (Rq)

$$Rq = Ra/1.11 \qquad \text{——————} \quad (5.7)$$

If Ra = 1 μm

1 μm = 0.04 μ inch

Then RMS = 0.04/1.11

Table 5.3.1 Average surface roughness (Ra) and root mean square (Rq) with the Fe-concentration in ZnO thin films

Fe (at.%) in ZnO	Average Roughness, Ra (nm)	Root Mean Square, Rq (nm)
0	112.9703	137.6061
5	56.7362	71.1655
10	45.7461	57.4253
15	31.5162	41.3735
20	17.8855	24.6177

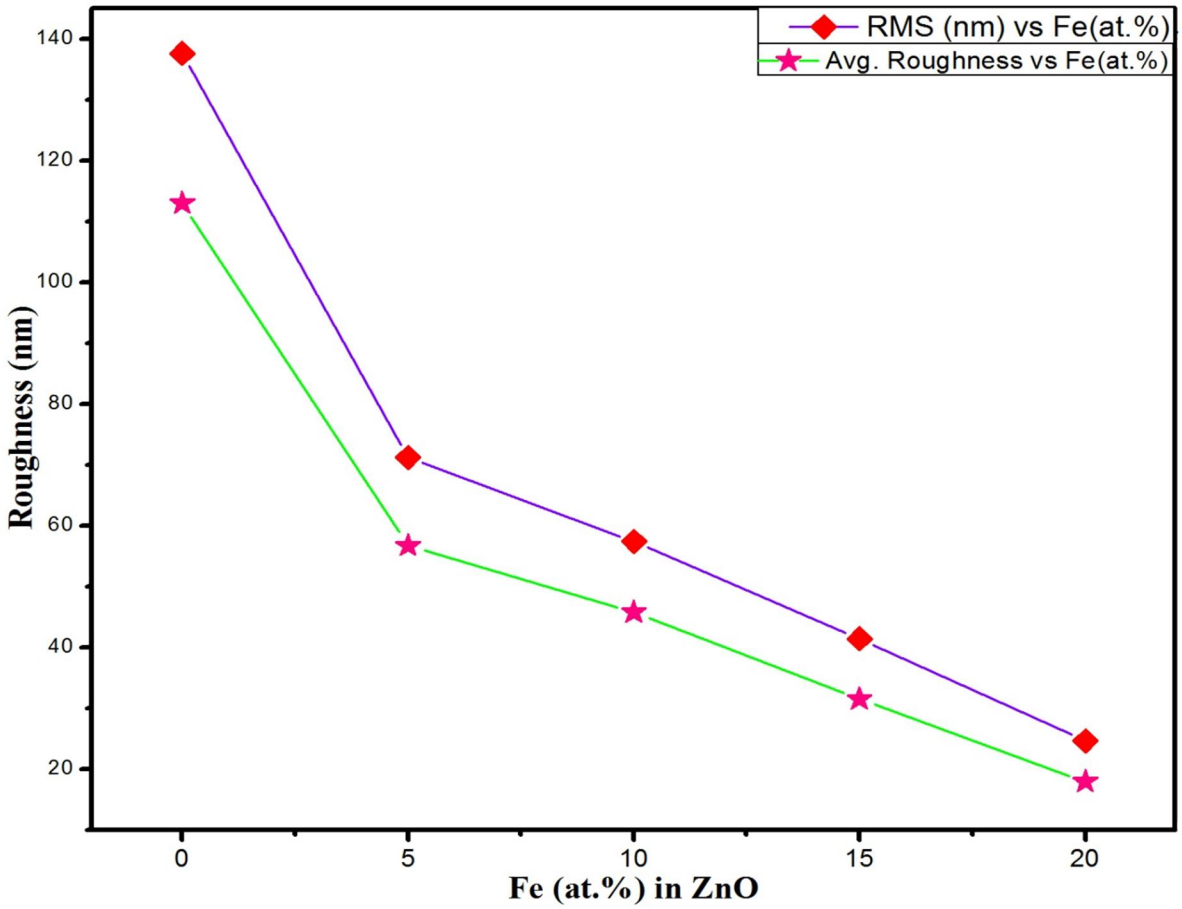

Figure 5.3.6 Variation of Roughness of thin films vs Fe (at.%) in ZnO

5.4 TEM Analysis

The Fe (10 at.%) doped ZnO particles annealed at 500 °C in ambient air and were analyzed by Transmission Electron microscope (TEM) Tecnai G2 20 S-TWIN. The results of low-resolution TEM characterizations are shown in figures 5.4.1. The particle size distribution were found out which are in the range of 28 – 38 nm and this was consistent with the FE-SEM results in which for Fe (10 at.%) the average particle size was 37.81 nm. The figure illustrates that growth mechanism has a tendency to hexagonal morphology. High-resolution TEM micrographs are presented in Figure 5.4.2 which show that all the nanoparticles are single crystalline in nature and are free from major lattice distortion or defects. The SAED (Selected Area Electron Diffraction) pattern of sample is shown in figure 5.4.2 was obtained by focusing the beam on some nanoparticles and this clearly indicates the single crystalline nature of each nanoparticle. The shape of the nanoparticles found to be qausi-spherical and the particle size is non-uniformly distributed, the reason may be the nanoparticles are aggregated together. Figure demonstrate nanoparticles have regular shape geometry and have a close similarity to symmetry of wurtzite structure. It was also confirmed that the nanocrystals are in wurtzite hexagonal phase from the XRD. The average particle diameter (size) was calculated from the low-resolution TEM data and using the standard software IMAGEJ.

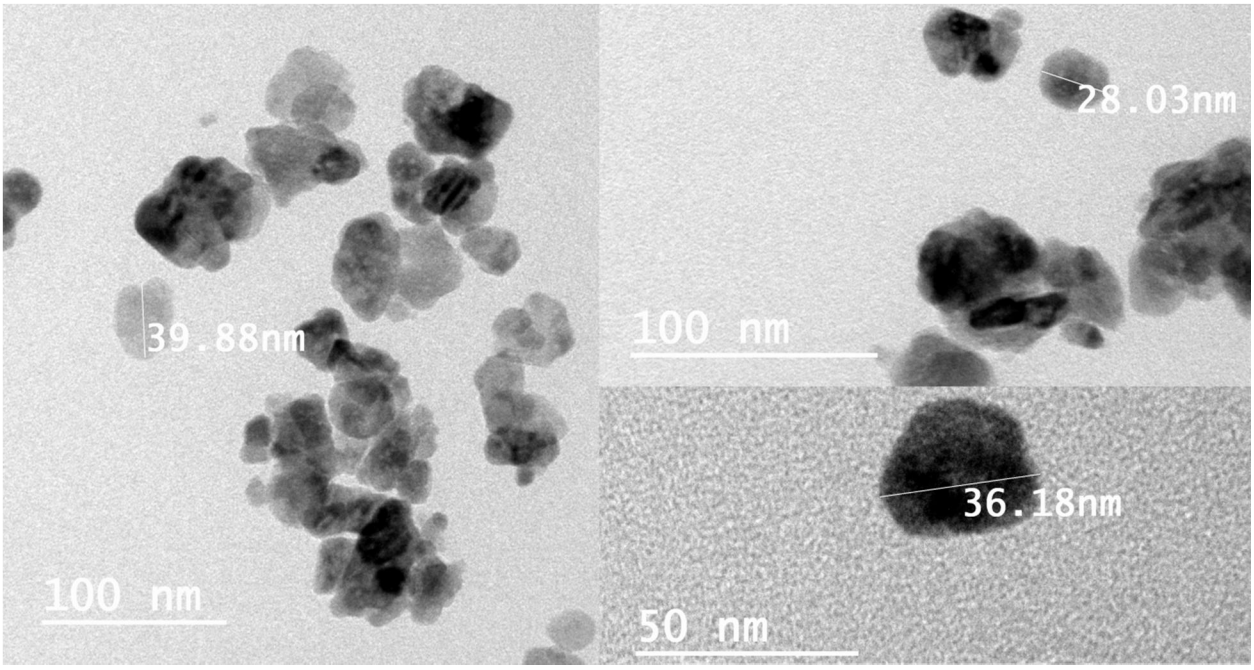

Figure 5.4.1 Low-resolution TEM micrograph of $Zn_{0.90}Fe_{0.10}O$

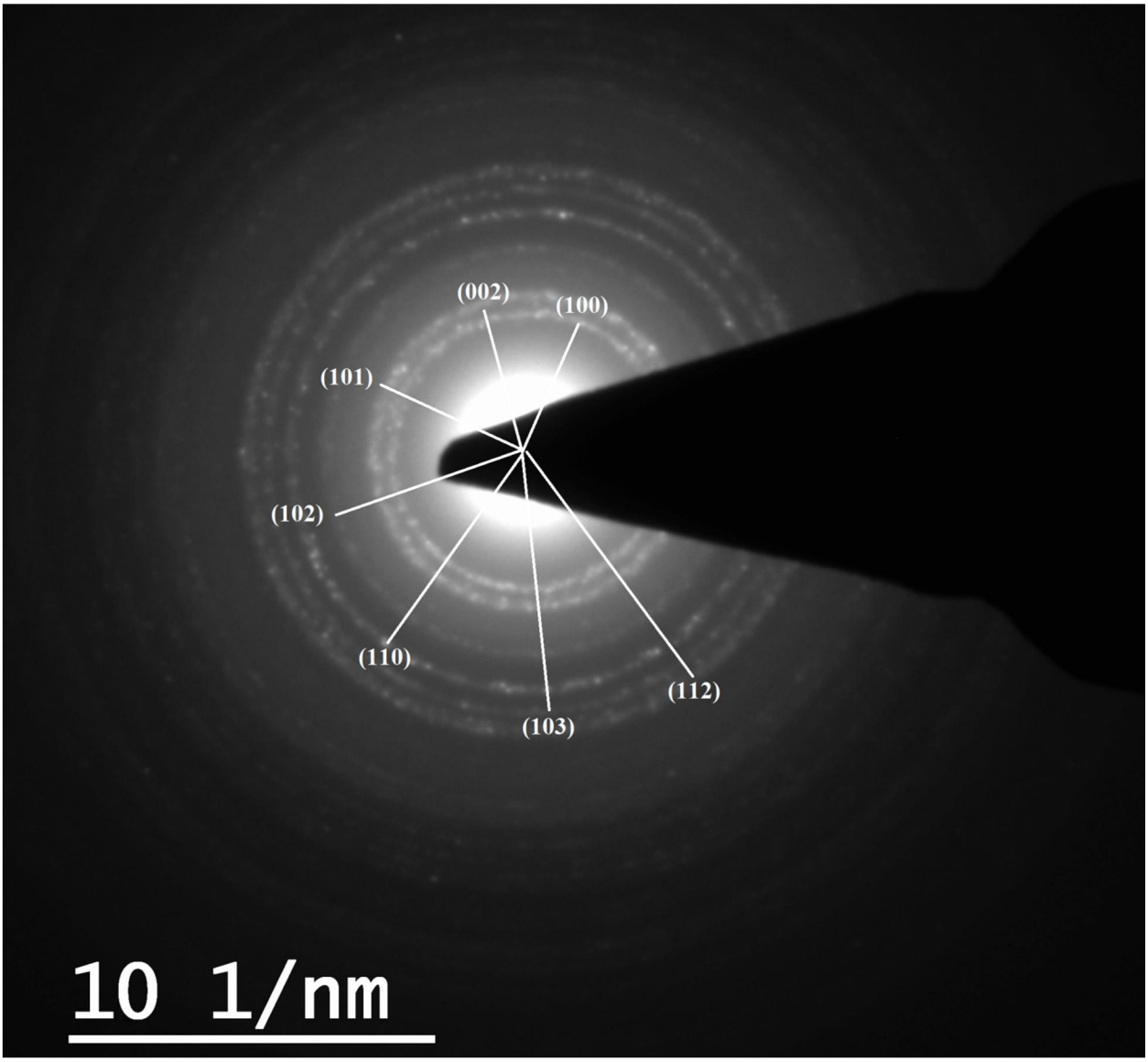

Figure 5.4.2 TEM showing (a) SAED pattern of $Zn_{0.90}Fe_{0.10}O$ nanoparticles showing single crystalline spot and the ZnO crystal planes

Figure 5.4.2 shows a typical SAED pattern of the $Zn_{0.90}Fe_{0.10}O$ nanoparticles annealed at 500 °C in ambient air. The figure consists of seven concentric diffuse broad rings (corresponding to zinc oxide lattice) over which dotted rings are superimposed. The broad diffuse rings indicates amorphous phase and dotted discontinuous rings indicates crystalline phase. This is characteristics of amorphous matrix having low dimensional crystalline phase. As marked in the figure, the seven characteristic concentric rings of d_{hkl} values are tabulated in the table 5.4.1 corresponds to the planes (100), (002), (101), (102), (110), (103) and (112) of ZnO crystal.

The high resolved HRTEM images of $Zn_{0.90}Fe_{0.10}O$ nanoparticles are shown in the figure 5.4.3 (a) showing the lattice fringes of the ZnO crystal and (b) *d* – spacing (lattice spacing). The lattice space (*d*) was calculated using IMAGEJ software, which is equal to 0.2619 nm. The *d* value of the plane (002) matches well with those d_{hkl} values calculated from XRD peaks and calculated values from SAED pattern.

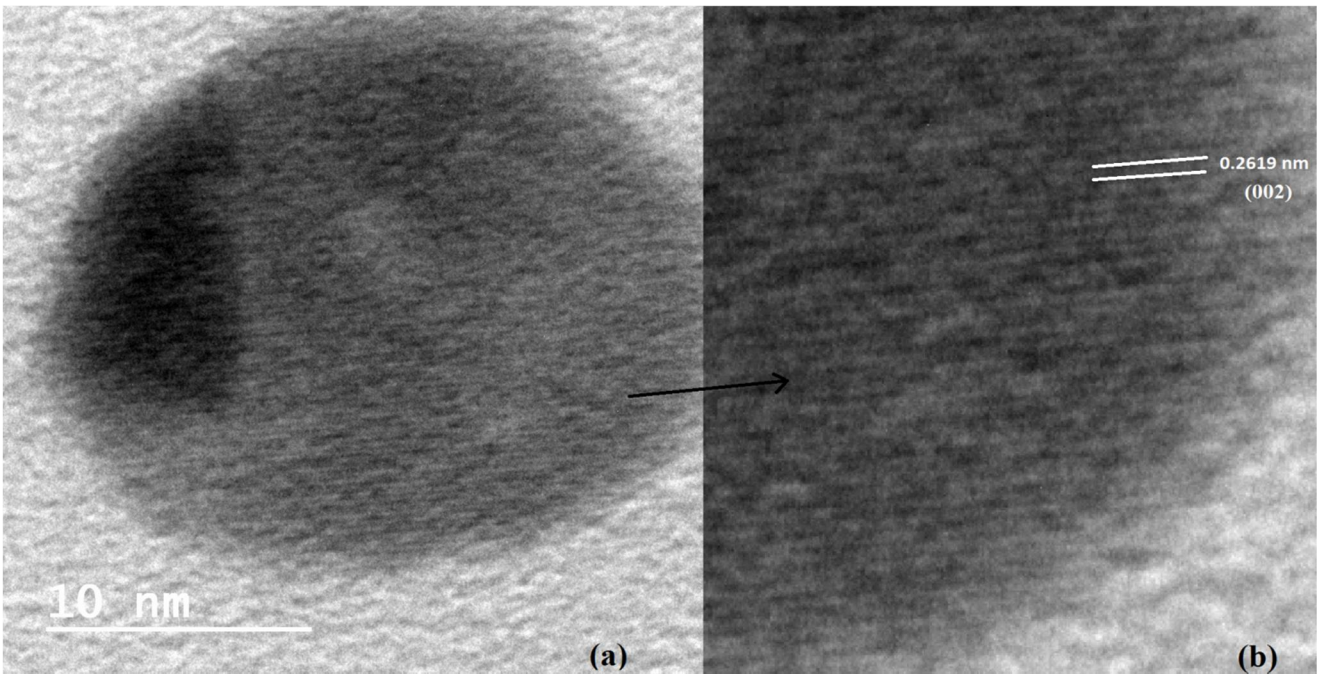

Figure 5.4.3 TEM images of $Zn_{0.90}Fe_{0.10}O$ showing (a) lattice fringes of crystal (b) Lattice spacing (*d*) and single crystalline nature of the nanoparticles

Table 5.4.1 Comparison of *d*–spacing values of XRD peaks and the SAED pattern values

ZnO Planes (*hkl*)	d_{hkl} (nm) (XRD peaks)	d_{hkl} (nm) (SAED pattern)
(100)	0.2817	0.2821
(002)	0.2603	0.2625
(101)	0.2478	0.2463
(102)	0.1911	0.1912
(110)	0.1627	0.1629
(103)	0.1477	0.1413
(112)	0.1379	0.1347

5.5 Magnetic characterization of the nanoparticles by SQUID

5.5.1 M-T curves of Fe Doped ZnO powder sample at (H=100 Oe)

Magnetic properties of all the powdered samples of $Zn_{(1-X)}Fe_XO$ ($0 \leq X \leq 20$) were studied by SQUID (Quantum Design MPMS XL Evercool) results. Magnetization M (emu/gm.) vs applied field H (Oe) experiment was performed at room temperature the applied magnetic field was in the range $\pm$ 50 KOe. The results were shown in the figure 5.5.3 Magnetization as a function of Magnetic field plot for different Fe concentrations. We can see that all the samples except Fe (0 at.%) show ferromagnetic behavior. All the samples have standard S-shape hysteresis loop at room temperature. The coercive field (H_c) of 70 Oe, 172 Oe, 248 Oe and 186 Oe and the remnant magnetization of (M_r) 0.04 emu/gm, 0.086 emu/gm., 0.135 emu/gm. and 0.0981 emu/gm. for the corresponding values at Fe concentration in ZnO of 5, 10, 15 and 20 at.%. The magnetization increases from Fe doping 0 at.% to 15 at.% and after that the value decreases. This is because for Fe 20 at.% secondary phases were formed such as FeO and $ZnFe_2O_4$ (spinel) which are well known anti-ferromagnetic materials.

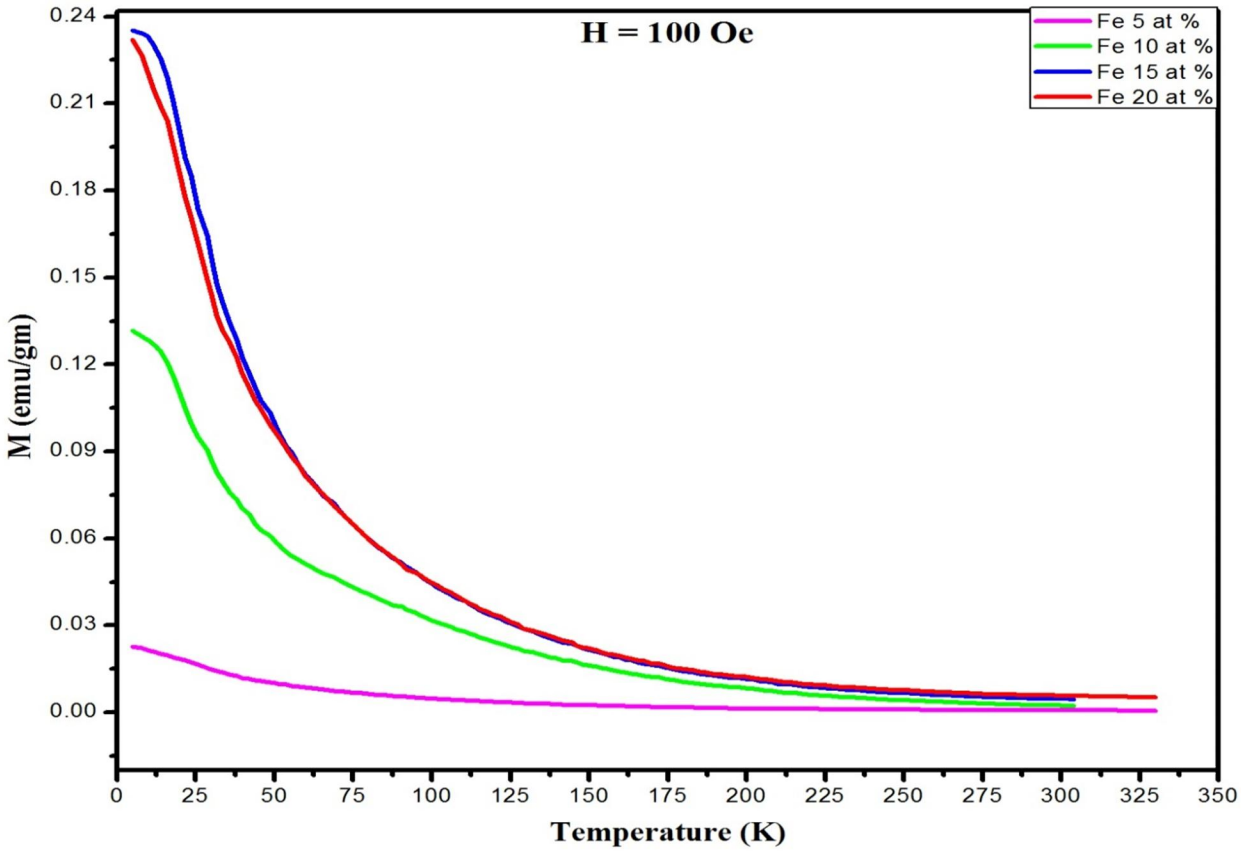

Figure 5.5.1 M-T curves of $Zn_{(1-X)}Fe_XO$ ($5 \leq X \leq 20$) at field H = 100 Oe

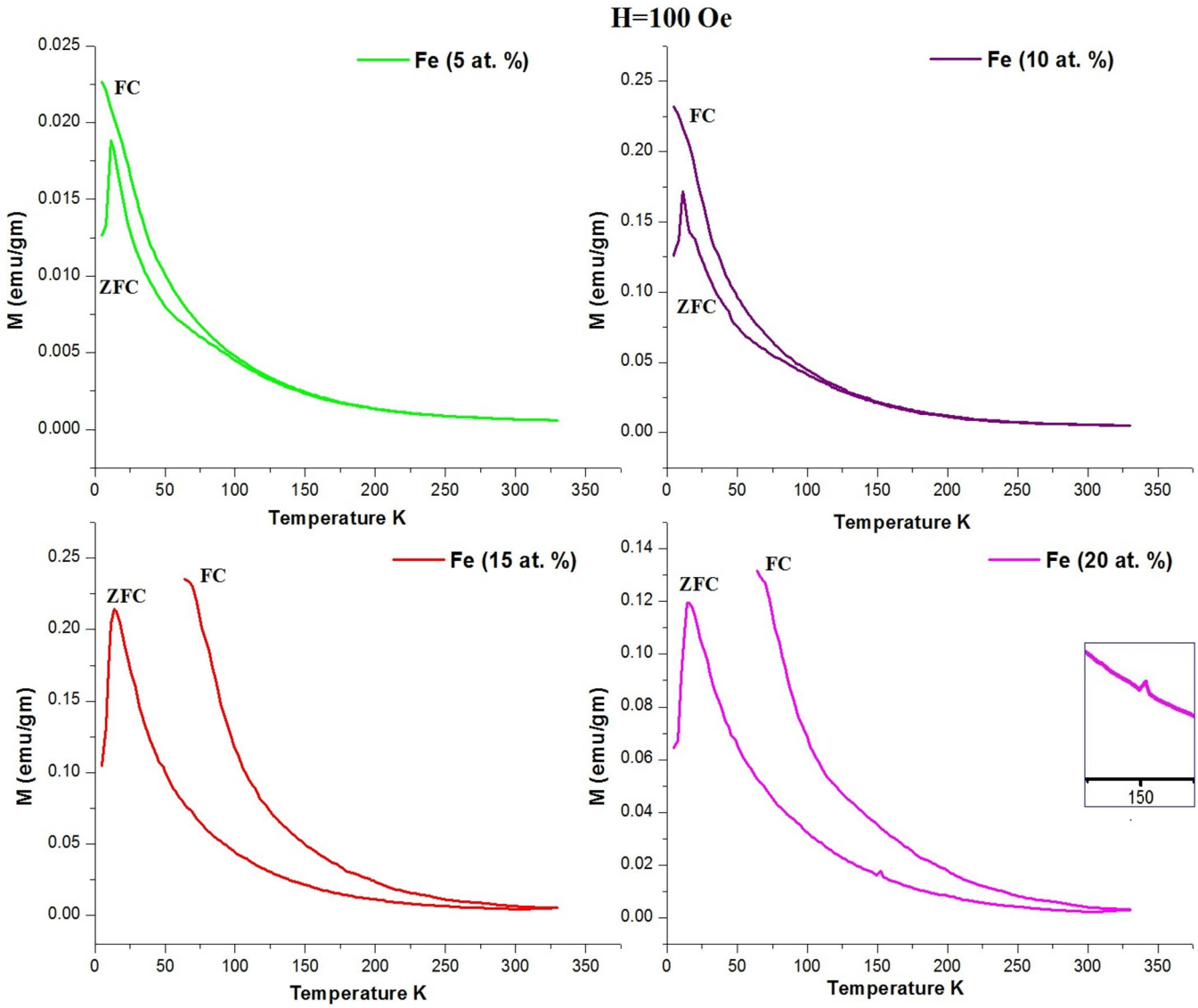

Figure 5.5.2 M-T (FC and ZFC) curves of $Zn_{(1-X)}Fe_XO$ ($5 \leq X \leq 20$)

We have studied the nature of M – T curves for the Fe doped ZnO powder samples at a constant magnetic field of H = 100 Oe and temperature in the range 5K to 330K.as we can see from the figure 5.5.2 M increases with the increasing Fe content in ZnO and also with decreasing temperature. The magnetization values of 10, 15, and 20 at.% Fe doped ZnO samples are more than that of 5 at.% Fe. Also the magnetization values are almost constant between the temperatures 150K and 330K, which clearly suggest ferromagnetic properties in the samples. We have expected the Curie temperature of all the four samples is well above the 300K, since there are no significant slope change in the M – T curves. It is also confirmed by the M – H curves at room temperature all the Fe doped ZnO powder samples still have clear hysteresis curve.

5.5.2 M-H curves of Fe doped ZnO powder sample at Room Temperature

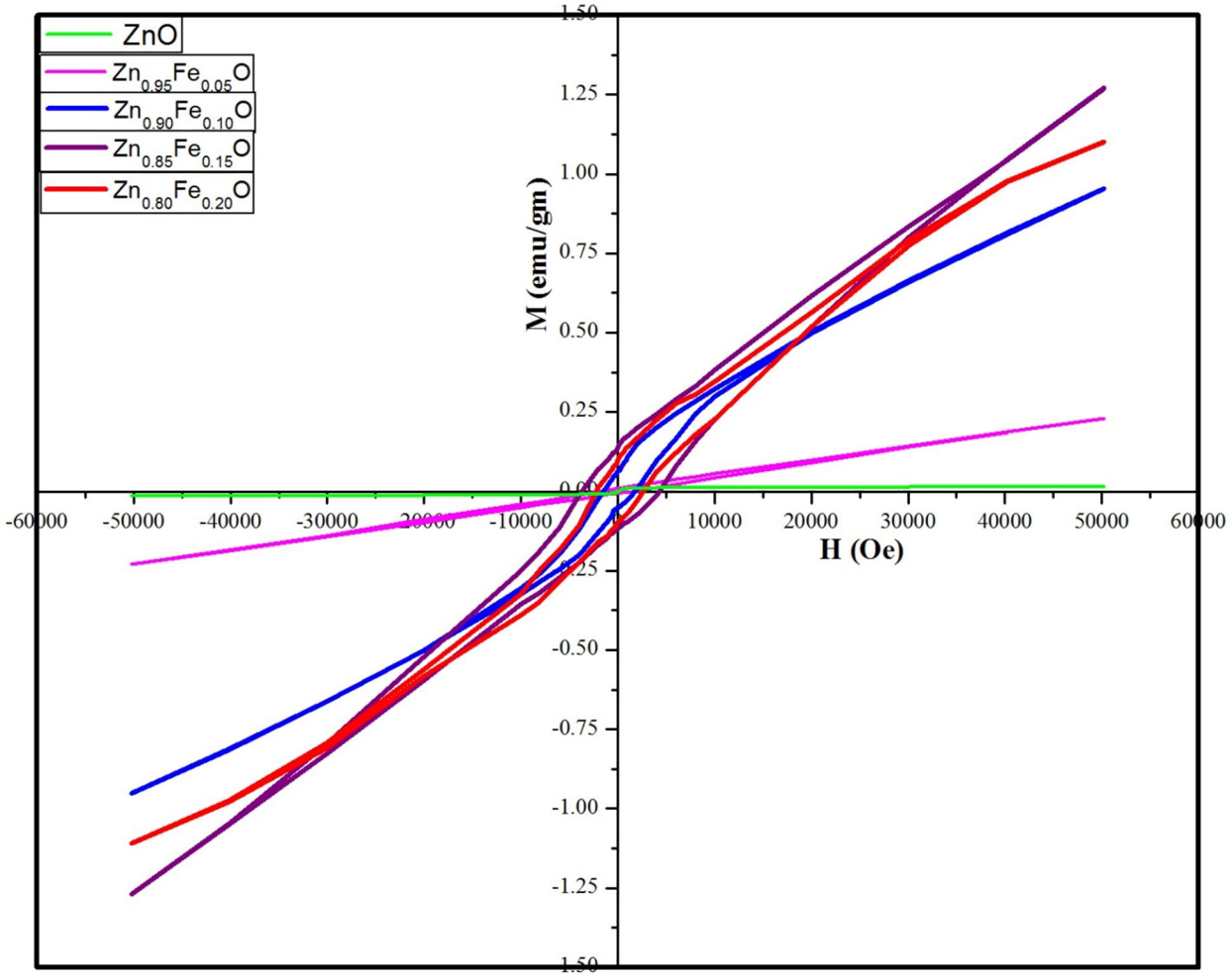

Figure 5.5.3 M-H curves of $Zn_{(1-X)}Fe_XO$ ($0 \leq X \leq 20$) at room temperature

Figure 5.5.2 shows the M-T curves for H=100 Oe in the temperature range of 5K-330K. From the figure we can see that magnetization value is positive supporting our M-H studies. All the curves show typical Curie-Weiss behavior. The magnetization decreases rapidly with increasing the temperature at high temperature. All the samples have concave curvature which is different from Weiss mean field prediction. This type of strong concave M-T behavior is often observed in carrier-localized regime, which can be understood by the Polaron-percolation theory reported by Sarma et al [19]. The M-T curves of Fe 20 at.% has a kink about 151 K as shown in in inset which is likely because of secondary phase transition, which could be related with Fe doping impurity in ZnO crystal lattice. This is also confirmed by XRD results at Fe 20 at.% secondary phases are present. This could be the reason of decrease in magnetization for the Fe 20 at.%.

Table 5.5.1 The H_c, M_r and M_s at $\pm$ **50 KOe** of $Zn_{(1-X)}Fe_XO$ ($0 \leq X \leq 20$) nanoparticles

Fe (at.%) in ZnO	H_c (Oe)	M_r (emu/gm)	M_s (emu/gm)
0	0	0	0.01423
5	70	0.04	0.2291
10	172	0.086	0.9541
15	248	0.135	1.2714
20	186	0.098	1.1099

The M_s of the samples were increased as Fe concentration increased, because of the increased number of magnetic ions is required to render ordered magnetic interaction as x increased. THE origin of RTFM in TM doped ZnO is still a controversy. Therefore ferromagnetism at room temperature in the Fe doped ZnO can be explained by substitution of Fe^{3+} ions for the Zn^{2+} ions in the tetrahedral position. According to RKKY theory ferromagnetism in the DMSs could be attributed to the increase in the exchange interaction between free delocalized carriers in the *s,p* cells (electron or hole from the valance band) in Zn and the localized *d* spins in the Fe. Hence the presence of free carrier interaction is necessary for ferromagnetism in DMSs.

The interactions between magnetic polarons and disordered defects may also play important role on the ferromagnetism in Fe doped ZnO thin films. The other possibility of ferromagnetism in DMSs is presence of impurities phases or secondary phases such as Fe clusters, Fe_2O_3 and Fe_3O_4 are well known ferromagnetic materials with Curie temperature more than 800K , There are no indications of secondary phases (FeO, Fe_2O_3, cluster Fe) in the XRD pattern. But the presence of precipitates or clusters small enough not detected by XRD analysis could not be excluded. Hence the FM at or above room temperature in the Fe doped ZnO thin films could not be alone explained in terms of presence of these possible secondary phases in the ZnO matrix.

5.6 Electrical characterization

5.6.1 Two probe setup

Electrical characterization of thin films was conducted by two probe setup and four-probe setup. Three samples of $Zn_{(1-X)}Fe_XO$ (X = 0, 5, 10) thin films were prepared. The V-I characteristics of the films were plotted using KEITLEY 2400 Source Measuring Unit. By varying the current (μA) output voltage (mV) was recorded.

Figure 5.6.1 show the V-I characteristics plots. We can see that in the ZnO thin films Ohmic behavior in the V-I curves were observed. The resistance of the films increases as the Fe-doping concentration increases. The increase in the resistivity could be due to increase in the induced stress which will reflect free charge carriers and reduce the mobility. The probable causes of increase in resistivity or decrease in conductivity are, first reason carrier traps at the grain boundaries which can entrap charge carriers and second reason might be formation of interstitial metal atoms and decrease in the oxygen vacancies due to Fe incorporation.

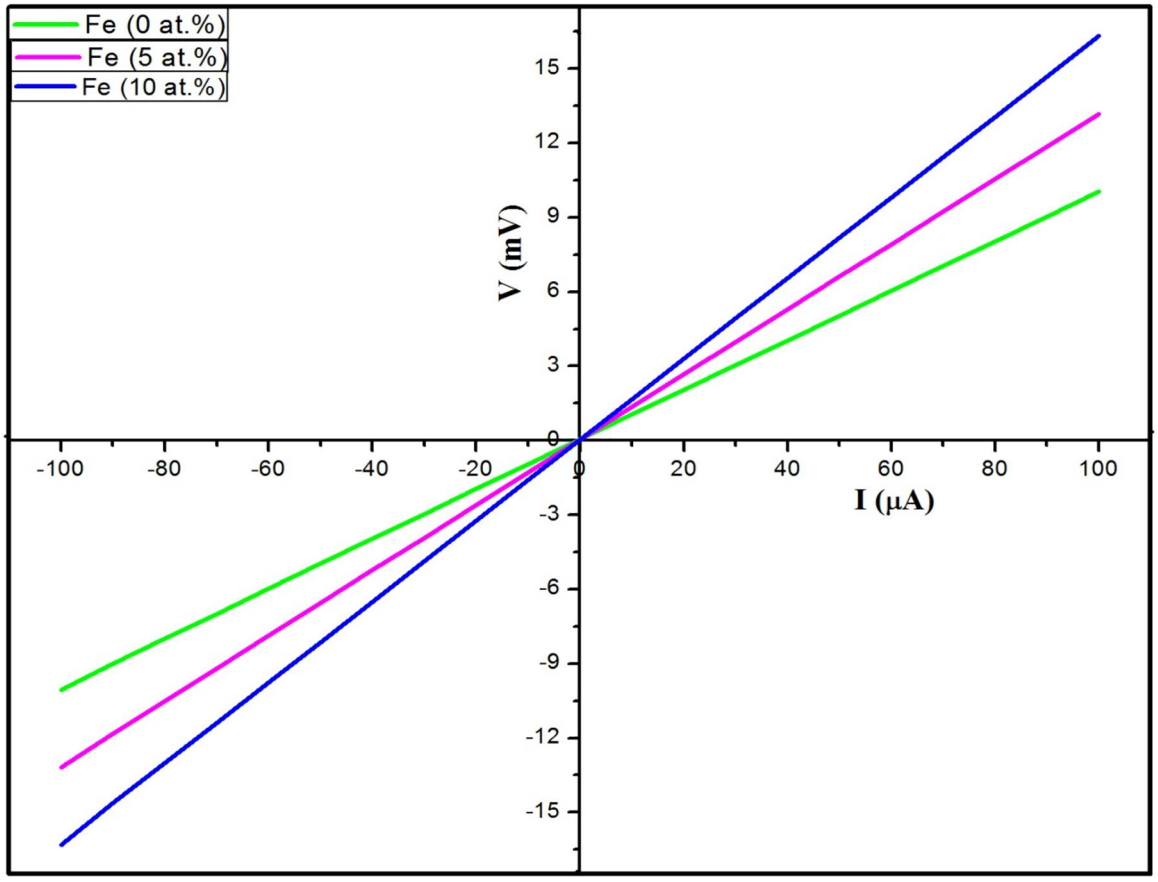

Figure 5.6.1 V-I characteristics of $Zn_{(1-X)}Fe_XO$ (X = 0, 5, 10) thin films

5.6.2 Four probe setup

The four probe experiment is used for the measurement of Resistivity (ρ) and Activation energy of the semiconductors. The resistivity (ρ) is calculated by using the following formula.

$$\rho_0 = \frac{V}{I} \times 2\pi S$$

By plotting the ($\log_{10}\rho$) vs (1000/T) curves and calculating their slopes will give Activation energy (E_g) in (eV).

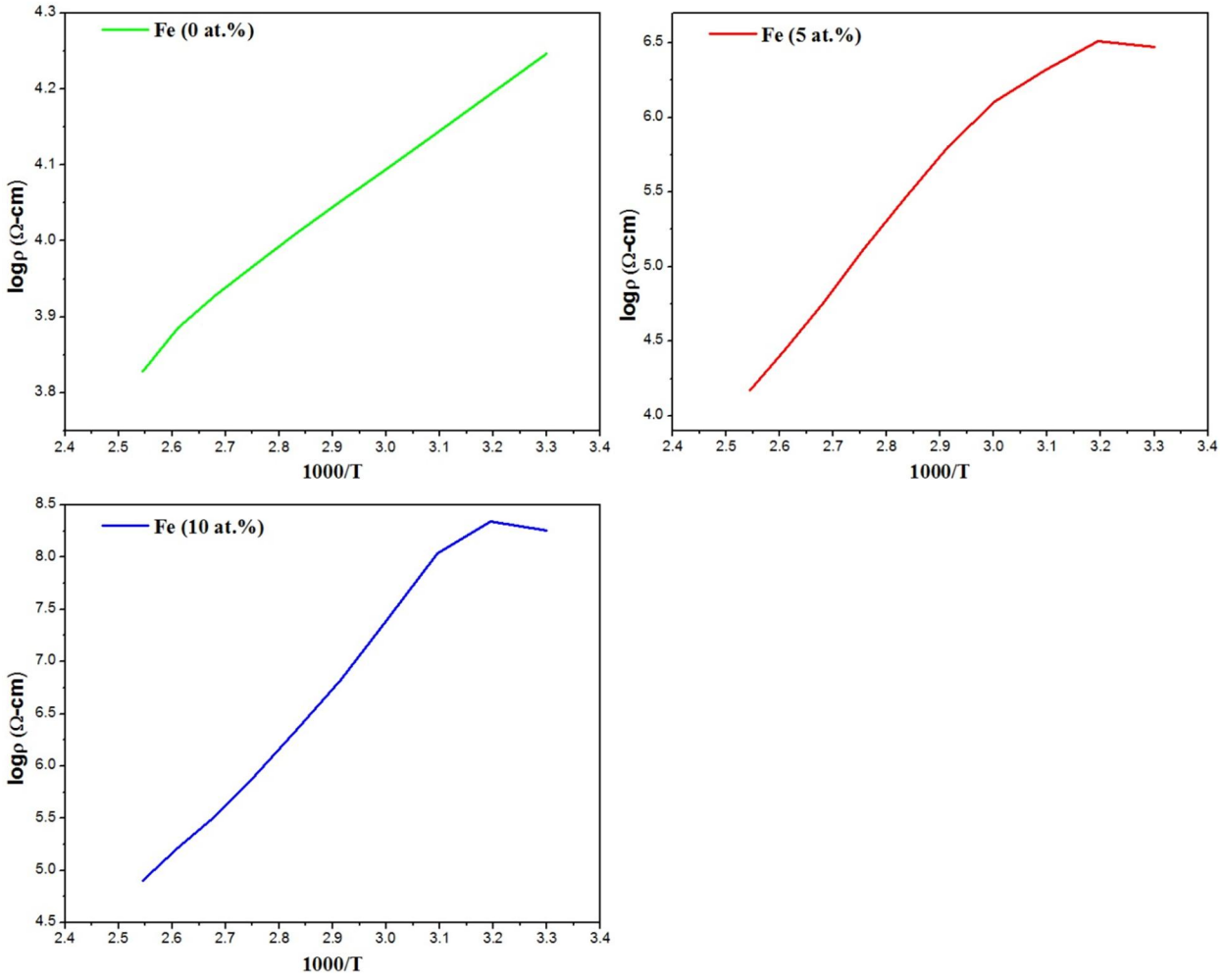

Figure 5.6.2 Temperature dependent of the electrical resistivity of $Zn_{(1-X)}Fe_XO$ (X = 0, 5, 10) thin films

The ($\log_{10}\rho$) vs (1000/T) plots are shown in the figure 5.6.2 as the Fe concentration increases the activation energy also increases. The two values of E_A are tabulated in the table 5.6.1. The increase in the activation energy may be distortion or disorder in the ZnO lattice. The charge carriers (electrons or holes) are scattered and because of this scattering the charge carriers need more energy to jump from valance band to conduction band.

Table 5.6.1 Resistance (R) values of thin films by two probe method

Fe (at.%) in ZnO	Resistance R (Ω)
0	99.896
5	132.105
10	163.297

Table 5.6.2 Electrical activation energy (E_A) and Resistivity (ρ) of $Zn_{(1-X)}Fe_XO$ (X = 0, 5, 10) thin films

Fe (at.%) in ZnO	Resistivity ρ (KΩ-cm)	Activation Energy E_A (eV)
0	2.803	0.214
5	1416.57	0.218
10	1907.404	0.545

6 CONCLUSIONS

Fe (0 – 20 at.%) doped ZnO thin films were successfully prepared by Sol-gel method. Thin films were synthesized on the glass substrate by using Spin coating equipment. The prepared samples were characterized XRD analysis which indicates presence of single phase Fe doped ZnO without any secondary phases except for Fe (20 at.%).Fe-SEM analysis showed thin films are uniform and have a homogeneous surface distribution of grains with average particle size in the range 28 – 57 nm. The EDX spectra showed Zn and Fe no other elements were present and no traces of other impurity elements were found in the EDX spectra. SQUID results indicate all samples have M–H loops in S-shaped and are characteristic of room temperature ferromagnetic (RTFM) behavior with a small saturation magnetization (M_s), after Fe (15 at.%) in ZnO M_s decreases. M – T curves (5K – 330K) show presence of secondary phases in $Zn_{0.80}Fe_{0.20}O$ samples other than that they exhibit ferromagnetic properties; hence we concluded that the curie temperature of the films is T_c > 330K. SPM topography analysis show, as Fe concentration increases in ZnO the roughness decreases. HRTEM results for $Zn_{0.80}Fe_{0.10}O$ revels particle size in the range 28 – 39 nm, which are in consistent with the FE-SEM results. SAED pattern consists of seven concentric diffuse broad rings and also the lattice spacing (*d*) along (002) plane was found to be 0.2619 nm, which in in comparable with the values from SAED pattern value (0.2625 nm) and XRD peaks (0.2603 nm) for the $Zn_{0.80}Fe_{0.10}O$ nanopowder. From the above results of XRD, FE-SEM, EDX, SQUID and HRTEM analysis we confirmed that Fe atom is substituted for Zn in ZnO lattice without altering the wurtzite hexagonal structure and the synthesized thin films exhibits room temperature ferromagnetism. The two probe experiments show increase in resistance (R) with Fe content in ZnO and four probe experiments show increase in resistivity (ρ) and activation energy (E_A) increases with Fe concentration in ZnO. Sol-gel method of producing DMS is simple, inexpensive more control over process parameters, efficient and allows wide range of different compositions on various substrates can be used to synthesis of DMSs. These Fe doped ZnO thin films may be potentially used for spintronics, solar cells, gas sensors, electrodes transducers and many electronics applications.

7 Future Scopes

After studying structural, electrical and magnetic properties of the Fe-doped ZnO thin films we come to know that there are several properties can be improved in the future for the synthesis of thin films.

To improve the nanostructure properties of the films there are few suggestions are given below

- Photoluminescence could be studied to know more about luminescence behavior of the films.
- Thin films could be prepared on different substrates such as ITO, silica wafer and Al_20_3 and the role of substrate matrix on the growth of films could be studied.
- Samples co-doped with different TM could be annealed at different temperatures and the variation in structural, electrical and magnetic properties can be analyzed.
- By using same precursor solution spin and dip coating methods could be employed to study the change in structural, optical, electrical and physical properties of the films.
- Electrical properties such as V-I characteristics, Hall measurement and impedance study could be studied for the prepared TM co-doped thin films.

References

[1] T. Dietl, H. Ohno: Ferromagnetism in III – V and II – VI semiconductor structure, Physica E9 (2001) 185 - 193

[2] Xu, H.Y., Liu X.L., Cui D.L., Li M. Jiang, M.H.: A novel method for improving the performance of ZnO gas sensors. Sens. Actuators, 2006; B 114, 301 - 307

[3] Bappaditya Pal, Soumen Dhara, P.K. Giri, D. Sarkar: Evolution of room temperature ferromagnetism with increasing 1D growth in Ni-doped ZnO nanostructures, Journal of Alloys and Compounds 647 (2015) 558 - 565

[4] C. Aydın, M.S. Abd El-sadekb, Kaibo Zheng, I.S. Yahiad, F. Yakuphanoglu: Synthesis, diffused reflectance and electrical properties of nanocrystalline Fe-doped ZnO via sol–gel calcination technique. Optics & Laser Technology 48 (2013) 447 - 452

[5] Shan FK, Yu YS: Band gap energy of pure and, Al-doped ZnO thin films. J Eur. Ceram. Soc. 2004; 24:1869 - 72

[6] Zayer NK, Greef R, Rogers K, Grellier AJC, Pannell CN: In situ monitoring of sputtered zinc oxide films for piezoelectric transducers. Thin Solid Films 1999;352:179 - 84

[7] Kyu-Hyun Bang, Deuk-Kyu Hwang: Effects of growth temperature on the properties of ZnO/GaAs prepared by metalorganic chemical vapor deposition. J Cryst. Growth 2003; 250:437 - 43

[8] Fukudome T, Kaminaka A, Isshiki H, Saito R, Yugo S, Kimura T.: Optical characterization of Er-implanted ZnO films formed by sol–gel method. Nuclear Instruments and Methods in Phys Research B 2003; 206: 287 - 90

[9] Lidia Armelao A, Monica Fabrizio F, Stefano Gialanella G, Fiorenzo Zordan Z.: Sol–gel synthesis and characterization of ZnO-based nanosystems. Thin Solid Films 2001; 394:90 - 6

[10] Puspharajah P, Radhakrishna S.: Transparent conducting lithium-doped nickel oxide thin films by spray pyrolysis technique, Mater. Sci. Eng. 1997; 32:3001 - 6

[11] Lamia Znaidi: Sol-gel-deposited ZnO thin films: A review, Mater. Sci. Eng. B 174, (2010) 18 - 30

[12] Yüksel Köseoğlu: Rapid synthesis of room temperature ferromagnetic Fe and Co co-doped ZnO DMS nanoparticles, Ceramics International 41 (2015) 11655 - 11661

[13]D. Karmakar, S.K.Mandal, R.M. Kadam, P.L. Paulose, A.K. Rajarjan, T.K. Nath, A.K. Das, I. Dasgupta, G.P. Das: Ferromagnetism in Fe-doped ZnO nanocrystals: Experiment and theory. Phys. Rev. B 75, (2007) 144404

[14] L. J. Fu, H. Liu, C. Li, Y. P. Wu, E. Rahm, R. Holze, and H. Q. Wu.: Electrode Material for Lithium Secondary Batteries Prepared by Sol-gel Method, Prog. Mater. Sci. (2005), vol. 50, pp. 881 - 928

[15] T. Dietl, H. Ohno, P. Kossacki, N. Akiba, F. Matsukura, J. Cibert, D. Ferrand, A. Wasiela. Ferromagnetism induced by free carriers in p-type structures of diluted magnetic semiconductors, Science 287 (2000) 1019

[16] K. Sato, H. Katayama-Yoshida, Jpn. First-principles material design and perspective on semiconductor spintronics materials. Physica B 404 (2009) 5237 - 5243

[17] K. Ueda, H. Tabata, T. Kawai: Fabrication of the low-resistive p-type ZnO by codoping method Physica B 302–303 (2001) 140 - 148

[18] S.A. Wolf, D.D. Awschalom, R.A. Buhrman, J.M. Daughton, S. von Molnaar, M.L. Roukes, A.Y. Chtchelkanova, D.M. Treger, Science 294 (2001) 1488

[19] I. Zutic, J. Fabian, S. Das Sarma, Spintronics: Electron spin coherence, entanglement, and transport Rev. Mod. Phys. 76 (2004) 323

[20] Rosari Saleh, Suhendro Purbo Prakoso, Adel Fishli: The influence of Fe doping on the structural, magnetic and optical properties of nanocrystalline ZnO particles, Journal of Magnetism and Magnetic Materials 324 (2012) 665 - 670

[21] Huilian Liu1, Jinghai Yang, Yongjun Zhang, Lili Yang, Maobin Wei and Xue Ding: Structure and magnetic properties of Fe - doped ZnO prepared by the sol-gel method. J. Phys.: Condens. Matter 21 (2009) 145803(4pp)

[22] Muneer M. Ba-Abbad , Abdul Amir H. Kadhum , Abu Bakar Mohamad , Mohd S. Takriff , Kamaruzzaman Sopian: Visible light photocatalytic activity of Fe^{3+} - doped ZnO nanoparticle prepared via sol–gel technique. Chemosphere 91 (2013) 1604 - 1611

[23] Debjani Karmakar, S. K. Mandal , R. M. Kadam , P. L. Paulose, A. K. Rajarajan, T.K. Nath, A. K. Das, I. Dasgupta and G. P. Das: Ferromagnetism in Fe-doped ZnO Nanocrystals: Experimental and Theoretical investigations. project SR/S2/CMP-19/2004

[24] Mariani A. Ciciliati, Marcela F. Silva, Daniela M. Fernandes, Mauricio A.C. de Melo, Ana Adelina W. Hechenleitner, Edgardo A.G. Pineda: Fe-doped ZnO nanoparticles: Synthesis by a modified sol–gel method and characterization. Materials Letters 159 (2015) 84 - 86

[25] A. Goktas, I.H. Mutlu, Y. Yamada: Influence of Fe-doping on the structural, optical, and magnetic properties of ZnO thin films prepared by sol–gel method. Superlattices and Microstructures 57 (2013) 139 - 149

[26] Z.C. Chen, L.J. Zhuge, X.M. Wu, Y.D. Meng, Thin Solid Films 515 (2007) 5462

[27] Changzheng Wang, Zhong Chen, Ying He, Lanying Li, Dong Zhang, Appl. Surf.

Sci. 255 (2009) 6881

[28] G. Vijayaprasath, R. Murugan, S. Asaithambi, P. Sakthivel, T. Mahalingam, Y. Hayakawa, G. Ravi: Structural and magnetic behavior of Ni/Mn co-doped ZnO nanoparticles prepared by co-precipitation method Ceramics International 42 (2016) 2836 - 2845

[29] Y. Köseoğlu: PEG- assisted hydrothermal synthesis and characterization of $Co_{0.1}Zn_{0.9}O$ DMS nanoparticles, J. Magn. Magn. Mater. 373 (2015) 195 – 199.

[30] J.J. Beltran, A. Pannoose, C.A. Barrero: Evidence of FM signal enhancement in Fe and Co codoped ZnO nano particles by increasing superficial Co^{3+} content, J. Phys. Chem. C 118 (2014) 13203 – 13217.

[31] Sheng, X., Zhao, Y., Zhai, J., Hiang, L., Zhu, D.: Electro-hydrodynamic fabrication of ZnO-based dye sensitized solar cells. Appl. Phys. 2007; A 87, 715 – 71.

[32] D.D. Sarma, E.H. Hwang, A. Kaminski: How to make semiconductors ferromagnetic: a first course on spintronics, Solid State Communications 127 (2003) 99 – 107.

[33] M.A. Awad, A.M. Ahmed, V.O. Khavrus, E.M.M. Ibrahim: Tuning the morphology of ZnO nanostructure by in doping and the associated variation in electrical and optical properties, Ceramics International 41 (2015) 10116 – 10124.

[34] T. Touama, F. Boudjouan, A. Chelouche, S. Khodja, M. Dehimi, D. Djouadi,J. Solard, A. Fischer, A. Boudrioua: Effect of silver doping on the structural, morphological, optical and electrical properties of sol-gel deposited nanostructured ZnO thin films, Optik 126 (2015) 5548 – 5552.

[35] ulm university, Research on and with Scanning Force Microscopy, Retrieved from http://wwwex.physik.uni-ulm.de/afmweb/

[36] Hong Kong Baptist University, Surface Analysis & Material Characterization Laboratory, Retrieved from http://sml.hkbu.edu.hk/fesem.html

[37] Jeevan Jadhav, Somnath Biswas: Shape-controlled magnetic nanoplatelets of Ni-doped ZnO synthesized via a chemical precursor, Journal of Alloys and Compounds 664 (2016) 71 – 82.

[38] Bappaditya Pal, D. Sarkar, P.K. Giri: Structural, optical and magnetic properties of Ni doped ZnO nanoparticles: Correlation of magnetic moment with defect density, Applied Surface Science 356 (2015) 804 – 811.

[39] A. El Amiri, R. Moubah, F. Lmai, M. Abid, N. Hassanain, E.K. Hlil, H. Lassri: Probing magnetism and electronic structure of Fe-doped ZnO thin film, Journal of Magnetism and Magnetic Materials 398 (2016) 86 – 89.

[40] Jonghyun Lee, Wonjoon Choi, Chaeok Kim, Jinpyo Hong: Electrical and Optical Properties of a n-Type ZnO Thin Film Deposited on a Si Substrate by Using a Double RF Co-Sputtering Method, Journal of the Korean Physical Society, Vol. 49, No. 3, September 2006, pp. 1126 - 1129.

[41] Kamal Baba, Claudia Lazzaroni, Mehrdad Nikravech: ZnO and Al doped ZnO thin films deposited by Spray Plasma: Effect of the growth time and Al doping on microstructural, optical and electrical properties, Thin Solid Films 595 (2015) 129 –135.

[42] Emrah Sarica, Vildan Bilgin: Structural, optical, electrical and magnetic studies of ultrasonically sprayed V doped ZnO thin films, Surface & Coatings Technology 286 (2016) 1–8.

[43] M. Shatnawia, A.M. Alsmadi, I. Bsoul, B. Salameh, G.A. Alna washi F. Al-Dweri, F. El Akkad: Magnetic and optical properties of Co-doped ZnO nanocrystalline particles, Journal of Alloys and Compounds 655 (2016) 244 – 252.

[44] Bappaditya Pal, Soumen Dhara, P.K. Giri, D. Sarkar: Room temperature ferromagnetism with high magnetic moment and optical properties of Co doped ZnO nanorods synthesized by a solvothermal route, Journal of Alloys and Compounds 615 (2014) 378 – 385.

[45] Pooja Dhiman, Khalid Mujasam Batoo, R.K. Kotnala, Jagdish Chand, M. Singh, Room temperature ferromagnetism and structural characterization of Fe,Ni co-doped ZnO nanocrystals, Applied Surface Science 287 (2013) 287 – 292.

[46] A. Franco Jr. T.E.P. Alves: Room temperature ferromagnetism in combustion reaction prepared iron-doped zinc oxide nanoparticles, Materials Science in Semiconductor Processing 16 (2013) 1804 – 1807.

[47] F. Pan, C. Song, X.J. Liu, Y.C. Yang, F. Zeng: Ferromagnetism and possible application in spintronics of transition metal doped ZnO films, Materials Science and Engineering R 62 (2008) 1 – 35.

[48] G. Vijayaprasath, R. Murugan, T. Mahalingam, Y. Hayakawa, G. Ravi: Preparation of highly oriented Al:ZnO and Cu/Al:ZnO thin films by sol-gel method and their characterization, Journal of Alloys and Compounds 649 (2015) 275 – 284.